

Instituto Tecnológico y de Estudios Superiores de Monterrey

Campus Monterrey

School of Engineering and Sciences



Development of a DC-DC converter-based balancing system for Lithium-ion battery cells based on State of Power reference

A thesis presented by

Abraham Alberto Martínez Barrón

Submitted to the
School of Engineering and Sciences
in partial fulfillment of the requirements for the degree of

Master of Science

In

Energetics Engineering

Monterrey Nuevo León, June 15th, 2021

Instituto Tecnológico y de Estudios Superiores de Monterrey

Campus Monterrey

School of Engineering and Sciences

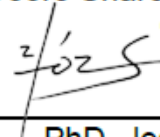
The committee members, hereby, certify that have read the thesis presented by Abraham Alberto Martínez Barrón and that it is fully adequate in scope and quality as a partial requirement for the degree of Master of Science in Energetics Engineering.




PhD. Gerardo Escobar Valderrama
Tecnológico de Monterrey
School of Engineering and Sciences
Principal Advisor



PhD. Ricardo Schacht
John Deere Shared Services
Co-advisor



PhD. Jesús Valdez
Tecnológico de Monterrey
School of Engineering and Sciences
Committee Member



Dr. Rubén Morales Menéndez
Dean of Graduate Studies
School of Engineering and Sciences

Monterrey Nuevo León, June 15th, 2021

Declaration of Authorship

I, Abraham Alberto Martínez Barrón, declare that this thesis titled, “Development of a DC-DC converter-based balancing system for Lithium-ion battery cells based on State of Power reference” and the work presented in it are my own. I confirm that:

- This work was done wholly or mainly while in candidature for a research degree at this University.
- Where any part of this thesis has previously been submitted for a degree or any other qualification at this University or any other institution, this has been clearly stated.
- Where I have consulted the published work of others, this is always clearly attributed.
- Where I have quoted from the work of others, the source is always given. With the exception of such quotations, this thesis is entirely my own work.
- I have acknowledged all main sources of help.
- Where the thesis is based on work done by myself jointly with others, I have made clear exactly what was done by others and what I have contributed myself.

Abraham Alberto Martínez Barrón
Monterrey Nuevo León, June 15th, 2021

Dedication

Dedicated to my fiancée and my parents, thanks for all your unconditional confidence, support, patience, and encouragement. You were my main motivation for pushing through this work.

Acknowledgments

I would like to express the deepest appreciation to my principal advisor, PhD. Gerardo Escobar, and to my co-advisor, PhD. Ricardo Schacht. Without their guidance and persistent help, this research project would not have been possible.

I am also grateful for the support that John Deere has provided me to cover my tuition, as well as for assisting me with the tools required for this assignment. In addition, I thank Tecnológico de Monterrey for allowing me to be part of the students of the Masters in Science in Energetics Engineering, as well as for providing the right environment for academic growth.

Development of a DC-DC converter-based balancing system for Lithium-ion battery cells based on State of Power reference

by

Abraham Alberto Martínez Barrón

Abstract

In recent years, Li-ion battery packs have become a major component of new technologies like energy storage systems and electric vehicles. Due to the safety limitations inherent to Li-ion battery cells, these packs need to be operated under precise voltage, temperature, and current conditions, which are variables supervised by a BMS. Depending on the application, battery packs are often comprised of several individual cells. However, each battery cell has slight variations, which can lead to performance and service life issues. This problem is addressed by implementing different types of balancing systems. Nevertheless, current methodologies face several limitations, such as a low energy efficiency for passive systems and high costs and complexity for active circuits. A new balancing system, consisting of the combination of a modular active DC-DC converter-based topology, a multi-factor balancing algorithm, and a control strategy for balancing current based on SoP, is developed in this research project. The resulting system can expand the runtime of the battery pack, as the energy is distributed better among cells. Besides, the energy that can be injected into the battery pack during charging has also been increased, as the excess of energy is moved from overcharged cells to the rest before anyone of them reaches its top voltage.

Figure index

Figure 1. (a) Thevenin-, (b) Impedance-, and (c) Runtime-based ECMs.....	8
Figure 2. De-coupled ECM by Chen and Rincon-Mora [22].	9
Figure 3. Classification of active and passive battery balancing and equalization methodologies [18], [12], [15].	11
Figure 4. Typical fixed shunt Resistors topology (a) and Modified Zener-fixed shunt resistors topology (b) [18].	13
Figure 5. Switched shunt resistor topology [12].	14
Figure 6. Typical switched capacitors topology [15].	15
Figure 7. Switched capacitors with double tier topology (a) and Circle patch switched capacitors topology (b) [12].	16
Figure 8. Single switched capacitor topology [15].	16
Figure 9. Basic transformer topology [15].	18
Figure 10. Multiple secondary windings topology [15] (a) and Multiple simple transformers topology [12] (b).	19
Figure 11. (a) Shared low voltage bus topology, and (b) example of a dual-active-bridge DC-DC converter circuit [18].	20
Figure 12. Multiple DC-DC converter topology with transformer-based bus [4].	21
Figure 13. Switch matrix topology with a balancing DC-DC converter [12].	22
Figure 14. (a) CCCV charging profile, and (b) PCV charging profile	28
Figure 15. ECM selected for simulation purposes [22].	30
Figure 16. (a) Individual cell block and, (b) portion of battery pack comprised of individual cells and sensor blocks.	31
Figure 17. Elements of the proposed balancing system.	32
Figure 18. Basic layout of the proposed active balancing topology.	34
Figure 19. Flyback DC-DC converter schematic.	35
Figure 20. Structure of the LC filter.	37
Figure 21. (a) Control loop for the charging converter, and (b) control loop for the discharging converter.	39
Figure 22. SoP-based control loop.	40

Figure 23. Comparison between open-loop and closed-loop response of charging converter for a desired output of 4.2 V.	43
Figure 24. Comparison between open-loop and closed-loop response of the discharging converter for a desired output of 84 V.	44
Figure 25. Comparison between open-loop and closed-loop response of the resulting balancing current for a value of 0.5 A.	47
Figure 26. Algorithm for selection of cells that require a balancing operation.	50
Figure 27. Proposed balancing algorithm with safety checks.	51
Figure 28. Speed and torque of the EPA agricultural tractor driving cycle [53].	56
Figure 29. Power and current curves derived from the EPA agricultural tractor driving cycle.	56
Figure 30. Power profile obtained from the residential mower driving cycle.	57
Figure 31. (a) Cell terminal voltage when discharged under a reference pulsed current cycle, and (b) reference pulsed current discharge cycle.	72
Figure 32. Equivalent circuit cell model used for electrical parameter estimation.	73
Figure 33. (a) Cell terminal voltage when discharged under reference discharge current cycle, (b) reference discharge current cycle, and (c) cell SoC when discharged under reference discharge current cycle. Red dots limit section of curves corresponding to periods of discharge, while green dots limit section of curves corresponding to rest periods.	74
Figure 34. Initial estimation of (a) VOC and (d) series resistance R_0 against SoC. Initial values for (b) time constant 1, (c) time constant 2, (e) resistor R_1 , and (f) resistor R_2 are also shown.	75
Figure 35. Initial estimation of (a) VOC and (d) series resistance R_0 against SoC. (b) and (c) show the trajectories for time constants 1 and 2 after initial estimation under curve fitting against SoC, while (e) and (f) show the initial guess for R_1 and R_2	75
Figure 36. Initial estimation of (a) VOC, (b) time constant 1, (c) time constant 2, (d) series resistor R_0 , (e) resistance R_1 , and (f) resistance R_2 against SoC, considering a linear system.	76

Figure 37. Final parameters of (a) VOC, (b) series resistance R_0 , (c) time constant 1, (d) resistance 1, (e) time constant 2, and (f) resistance 2 against SoC, after design optimization.	77
Figure 38. Comparison of 1RC, 2RC, and 3RC models showing (a) cell voltage and (b) error percentage when the reference of the discharge pulse is applied to the system. .	79
Figure 39. Detail of the comparison of the cell voltage resulting from models with different RC branches.	79
Figure 40. RW current profile showing how current varies between 0 and 4 A at fixed intervals.	80
Figure 41. Comparison of 1RC, 2RC, and 3RC models showing (a) cell voltage and (b) error percentage when a random walk discharge profile is applied to the cells.	81
Figure 42. CCCV charger circuit. Solid lines represent electrical flow, while dashed lines represent information flow.	83
Figure 43. Battery pack comprising 3 individual cells connected to the passive balancing system, which includes a simple balancing algorithm.	84
Figure 44. Basic Stateflow™ balancing algorithm for passive balancing considering only VOC.	85
Figure 45. VOC of the three cells for the (a) unfiltered measurement, and (b) after LPF action of the sensor. Signals processed by the filter show very small variation when compared to each other.	87

Table index

Table 1. Comparison of Various Equivalent Cell Models.....	9
Table 2. Summary of advantages and disadvantages of balancing methods.....	24
Table 3. Cell parameters of the 1RC cell model after parameter estimation.	30
Table 4. Common parameters for the two DC-DC converters.....	35
Table 5. Specific parameters for the charging converter.	36
Table 6. Specific parameters for the discharging converter.	37
Table 7. Parameters for the PI controllers used in the simulations.	47
Table 8. Charging time and runtime results from simulations under passive and the proposed active balancing schemes compared to simulations without a balancing system.	59
Table 9. Energy results from simulations under different balancing schemes.....	60
Table 10. Energy results from simulations under passive and the proposed active balancing schemes compared to simulations without a balancing system.....	60
Table 11. Balancing results from simulations under different balancing schemes.	61
Table 12. Electrical parameters obtained from the electrical parameter estimation for a 3RC ECM model.	77
Table 13. Summary of comparison between 1RC, 2RC, and 3RC models under the reference of the discharge pulsed current.	80
Table 14. Summary of comparison between 1RC, 2RC, and 3RC models under RW discharge.....	82

Contents

Abstract.....	ii
Figure index	iii
Table index.....	vi
List of acronyms	ix
Chapter 1 Introduction.....	1
Chapter 2 Problem Formulation	5
2.1 Problem definition	5
2.2 Research questions	5
2.3 Objectives	6
2.4 Hypothesis	6
2.5 Theoretical framework	7
2.5.1 Battery cell modeling	7
2.5.2 Battery balancing background.....	10
2.5.3 Passive balancing methods.....	11
2.5.4 Active balancing methods	14
2.5.5 Balancing algorithms	22
2.5.6 Summary and trends	23
2.5.7 Remarks on current technologies.....	26
2.5.8 Charging profiles	27
2.6 System description – Case study.....	29
2.6.1 Mathematical model of Li-ion battery cell	29
2.6.2 Construction of battery pack.....	31
Chapter 3 Development	32
3.1 Proposed balancing system overview.....	32

3.2 Development of the balancing topology	32
3.2.1 Proposed balancing topology	33
3.2.2 Design of DC-DC converters.....	34
3.2.3 Design of LC filter.....	37
3.3 Proposed control loop.....	38
3.3.1 Design of PI controllers	40
3.3.2 Tuning of the PI controllers	41
3.4 Development of the balancing algorithm.....	47
3.4.1 Multi-factor cell selection algorithm (MFCSA)	48
3.4.2 Balancing factors.....	52
Chapter 4 Numerical evaluation of proposed system	54
4.1 Simulation environment	54
4.2 Simulation conditions.....	54
4.2.1 Charging profiles	54
4.2.2 Discharging profiles.....	55
4.2.3 Simulation cycle	57
4.2.4 Balancing schemes	58
4.2.5 Cell conditions.....	58
4.3 Simulation results	58
4.3.1 Analysis on charging and discharging times	58
4.3.2 Analysis on energy efficiency	59
4.3.3 Analysis on cell balancing	61
Chapter 5 Conclusions and future work	63
Chapter 6 Bibliography.....	66

List of acronyms

AC	Alternating current
BMS	Battery management system
CC	Constant current
CCCV	Constant current constant voltage
CV	Constant voltage
DBA	Distance-based algorithm
DC	Direct current
DG	Distributed generation
DPST	Double-pole single-throw
ECM	Equivalent circuit model
ECU	Electronic control unit
EPA	Environmental Protection Agency
ESS	Energy storage system
EV	Electric vehicle
MFCSA	Multi-factor cell selection algorithm
PCV	Pulsed constant voltage
PI	Proportional-integral
RC	Resistor-capacitor
RW	Random walk
SoC	State of charge
SoE	State of energy

SoH	State of health
SoP	State of Power
UAV	Unmanned aerial vehicle
VOC	Open-circuit voltage

Chapter 1

Introduction

Lithium based batteries have become the dominant power storage solution for a wide variety of applications [1]. After a heavy increment in the usage of Li-ion battery cells in recent years in most of all technologies, such as *electric vehicles* (EV), drones, cell phones, among others, and due to limitations in the natural resources and energy sources, it becomes of a great interest to maximize the performance and service life of battery packs through an adequate *battery management system* (BMS) [2], [3], [4]. Since this growing trend shows no signs of stopping, and as battery cells are made using finite resources like Lithium, Cobalt, Manganese or Nickel, it is important to guarantee their usage at their maximum capacity [5]. Clearly, this limited resources availability increases the cost of the battery cells and the pack itself, so costumers tend to be very critical of under-performing systems, especially in the segment of consumers electronics, and more recently in the EV market [6].

Depending on the application, battery packs are often comprised of several individual cells, which are then connected in series and/or parallel to satisfy the energy and power requirements of the machine or system [7]. Due to the safety limitations inherent to Li-ion battery cells, these packs need to be operated under precise voltage, temperature, and current conditions, which are variables supervised by a BMS. On one hand, operating below the voltage and charge limits of the cells can damage their internal structure permanently, accelerating their end of service life [2], [8], [9]. On the other hand, overvoltage or overcharging, as well as charging cells too quickly, need to be prevented as these conditions can lead to thermal runaway and other dangerous scenarios, such as sudden explosions [10], [11]. Regulating temperature is also a key feature of a BMS, as operating outside the safe limits can accelerate the effects of aging [12]. Failures of battery systems in devices such as cellphones, *unmanned aerial vehicles* (UAV) and EVs can bring in legal repercussions to the manufactures as they pose a serious risk to users [11]. Hence, adequate means to ensure uniform performance of the cells are required [9].

Moreover, the parameters and characteristics of each individual cell do not exactly match each other, a phenomenon that is often attributed due to limitations in the

manufacturing process [10], [3], [13]. Different capacities, self-discharging rates, and internal resistances can lead to stopping the flow of energy from a battery pack even when some cells still have some remaining energy, which is detrimental to the overall performance of the system and imposes a limit to the range of a vehicle for instance [6]. In the same way, stopping the charging process when only a portion of the cells have reached full charge limits the available system energy during online operation [10]. These situations can result in a diminished operational life of a single cell or a module [12]. As battery packs are often assembled as a set or modules, replacing a single cell is not a viable option for a customer, which increases the cost of repairing the electric system in a given application.

Several techniques and approaches to mitigate or control these effects have been proposed in the literature and are collectively known as battery pack balancing and equalization methods [14], [12], [15], [16]. An appropriate battery balancing method is crucial in the design of any BMS to ensure energy efficiency, adequate performance and prolonged battery pack life. The idea behind this reasoning is that, an adequate balancing system minimizes the impact on performance and on battery life caused by the small differences found across the individual cells inside a battery pack [8], [17]. As stated before, ensuring a homogeneous *state of charge* (SoC) through the cells in the pack can greatly improve the performance of the system. The balancing system ensures that aged cells are not stressed more than healthier cells, prolonging the service life of the whole battery pack.

These balancing technologies are designed to ensure that the pack operates under normal conditions at the pack, module, and individual cells levels. Balancing a battery, comprised of series-connected cells, implies the guarantee that the cells will have the same matched voltage. This is not needed when working with parallel-connected cells, as this configuration naturally ensures self-balancing [18]. In contrast, equalizing a battery pack is the process through which the SoC of the cells in a string is matched. These concepts can be better understood considering a system of water tanks connected in series. If the tanks have the same water level, then they will all be depleted at the same time after operation, without unused water remaining in the reservoirs. Battery balancing and equalization methods can be divided in passive and active approaches [4], [15]. The

first ones achieve balance through energy dissipation, while the second ones are able to move charge from one cell to another through different devices [12].

Nonetheless, present battery balancing and equalization methods face some limitations. While the passive technologies are able to keep costs low, they waste energy that could have been used to further lengthen the runtime of the machine or for other purposes, such as for powering up accessory loads [4]. Moreover, balancing methods such as passive dissipation can increase the temperature of the battery pack, thus increasing the need of cooling and potentially elevating the overall costs of the electrical system [19]. Moreover, balancing methods such as passive dissipation can increase the temperature of the battery pack, thus increasing the need of cooling and potentially elevating the overall costs of the electrical system [19]. Besides, the balancing times achieved through these methods do not support efficient online operation; in other words, they are not meant to be used while the battery pack is providing power to an application. Passive methods are only used during charging, which results in a battery pack that is only balanced when fully charged and subject to imbalance during discharge [12]. Even though active techniques shorten the balancing time and increase the energy efficiency of the overall system, their higher costs have limited their practical applications [20]. Comparative studies between different balancing circuits have shown a capacity increase and a lower deviation in cell parameters in packs that have been actively balanced as opposed to passively-balanced packs [14], [16]. Comparative studies between different balancing circuits have shown that packs actively balanced exhibit a capacity increase and a lower deviation in cell parameters, which is in contrast to passively-balanced packs [14], [16]. Therefore, further research on highly efficient and cost-effective designs is needed to avoid these limitations.

While the methods or systems to balance cells have been the subject of study of some authors, other researchers have focused their attention in developing algorithms to determine which cells need balancing, in the form of delivering excess energy to the pack or receiving more energy than other cells. Two common methods have been proposed based on either cell-voltage or SoC [14]. By inspecting a single measurement or estimation, the algorithm decides which cells require a balancing operation. While these algorithms are easy to implement, they face some severe limitations. On one hand, the external voltage of a cell may not represent accurately its SoC. On the other hand, as

SoC must be estimated, inaccuracies in the battery model may lead to erroneous approximation [21].

Currently, BMS commonly used in the industry are capable of implementing passive balancing with simple balancing algorithms, basing the selection of cells to balance purely on cell voltage or cell SoC difference [16], [21]. The hardware, comprising transistors, resistors, and controllers, is generally described in detail. There are also some BMS using more complex algorithms, which are, however, intellectually protected property and no detailed description is available to the public.

The present work will propose a new design of a BMS based on active balancing circuits with certain modifications to improve its efficiency and cost-effectiveness, coupled with a novel balancing algorithm to identify cells that required balancing, i.e., to identify cells that need to deliver energy to other cells or that need to accept an excess of energy. As a result of this research, a novel active balancing system is proposed. This active balancing system is based on novel DC-DC converter-based circuits and includes a selection algorithm referred to as *multi-factor cell selection algorithm* (MFCSA). Furthermore, simulations models are to be delivered in order to test the performance of traditional and novel methodologies. As the current literature already contains extensive and very mature information about Li-ion battery cell modeling, a revision of this information has not been included in this research [22]. Nevertheless, existing models will be implemented to create a simulation platform for the development of other balancing circuits and algorithms to be proposed in the future.

The rest of this thesis proposal is structured as follows. Chapter II defines the specific problem to be solved, presents the hypothesis to be tested, and provides the theoretical background for this work. In Chapter III, the DC-DC converter topology, the multi-factor cell selection algorithm and the control loop that conform the proposed balancing system are developed. Chapter IV presents the simulation results to validate the proposed solution to balance a 20-cell module with varying conditions that exemplify real scenarios. Chapter V presents the conclusions derived from this work and provides some ideas for future research.

Chapter 2

Problem Formulation

The following section presents the problem to be solved by the proposed balancing system and the hypothesis that directs this research. Theoretical background is also provided to further expand on current balancing systems and their limitations.

2.1 Problem definition

The problem to be solved is to design a balancing system, including both circuit and algorithm, suitable for different operational field and environmental conditions, characterized by a high energy efficiency and low implementation costs. This system is expected to perform well in harsh conditions, such as highly unpredictable driving cycles, high power demand, and rough environmental conditions. Energy efficiency, implementation costs and impact to battery pack service life will be the main criteria for the design. Although, cell modeling and characterization is not the target of this research, they will be performed to create a framework to develop and test the balancing systems under study. The analysis will be bounded to battery modules containing no more than 20 individual cells connected in series; however, similar theoretical principles can be applied to extend its applicability to larger modules.

This research will be focused on designing a balancing topology for series-connected cells as this configuration does not provide any natural balancing scheme [18]. In contrast, parallel-connected cells achieve balance and equalization naturally through their connections. As most battery packs are cooled through forced convection, temperature will be analyzed as a disturbance in the cell model. Temperature will be calculated using the models described by Lin et al. [23], and fed into the battery model and balancing algorithm to influence the decision for the selection of cells to balance, as well as to demonstrate the robustness of the balancing system.

2.2 Research questions

Some of the research questions that will be addressed in this investigation are the following:

- What are the energetic efficiencies, implementation costs, and balancing times of current balancing methods?
- How do balancing algorithms and circuitry affect battery pack service life?
- How does cell balancing algorithms affect the performance of the balancing system and how can they be improved?
- What are the current design opportunities for DC-DC converter-based balancing topologies?
- How can implementation costs of active balancing methods be kept low?

2.3 Objectives

General objective: Develop a new practical active DC-DC converter-based balancing topology and multi-factor balancing algorithm, capable of improving the battery pack service life, achieving high energy-efficiency and keeping implementation costs low, during the course of 1.5 years, by means of reviewing promising balancing schemes found in the literature, and then modifying them to improve certain characteristics.

Specific objectives:

- Develop a balancing algorithm achieving short balancing times, while keeping battery cells inside safe voltage, temperature and current limits under different scenarios.
- Develop a modular balancing topology based on active DC-DC converter schemes capable of keeping lower implementation costs.
- Analyze the proposed balancing system regarding efficiency, robustness, and reliability against different field conditions.

2.4 Hypothesis

Since existing balancing systems are not able to achieve high energy efficiency with low implementation costs, the following hypotheses are presented:

- A modular DC-DC converter-based balancing topology achieves higher energy efficiency while maintaining low implementation costs.

- A multi-factor balancing algorithm can improve the performance of the battery pack during operation, since excessive cell stress due to inconsistencies in the algorithm can be avoided.
- Coupling a multi-factor balancing algorithm with an active DC-DC converter-based circuit results in a robust balancing system.
- If the balancing system operates during online operation, then it will prolong the battery pack service life, as it will keep cells under homogeneous conditions of operation.

2.5 Theoretical framework

This section presents the background to understand basic concepts behind Lithium-ion battery cells, as well as the idea behind balancing and equalization systems. Current methods found in the literature are presented and classified into passive or active topologies, depending on whether they dissipate or redistribute excess energy, respectively. At the end of this section, a summary and remarks of the covered technologies is presented.

2.5.1 Battery cell modeling

Battery cells are analyzed by using different models found in current literature that generally fall into one of three categories: electro-chemical, mathematical or *equivalent circuit models* (ECM) [24], [25], [22]. Electrochemical models involve a system of coupled time-variant spatial partial differential equations to accurately represent the behavior of the cells. However, they require days of simulation time, complex numerical algorithms, and battery-specific information that is often of intellectual property nature. They are mainly used for optimization of physical design aspects of batteries. Besides, pure mathematical models are often too abstract to provide a practical meaning but can predict system-level behavior such as battery runtime, efficiency or capacity. Nevertheless, they do not offer any I-V information important for circuit simulation and are often application-dependent.

ECMs use a combination of voltage sources, resistors, and capacitors to simulate the behavior of battery cells during co-simulation with other electronic components. As

these models can be easily connected to other electronic circuitry, they are of special use in balancing and equalization simulations. Different ECM exist in the literature, each with their own advantages and disadvantages. Figure 1 shows three different ECM approaches briefly described in this work.

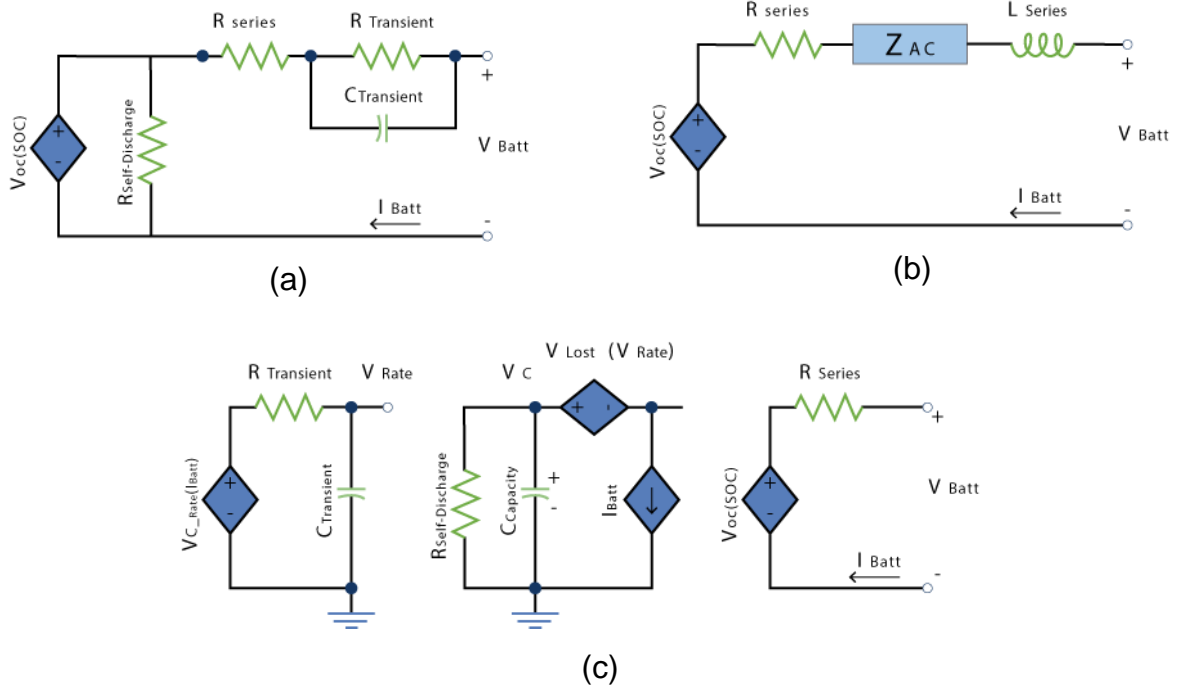


Figure 1. (a) Thevenin-, (b) Impedance-, and (c) Runtime-based ECMs.

“Thevenin-based electrical models” [26], [27], [28] can predict battery response to transient load events at a given SoC, by assuming the *open-circuit voltage* (VOC) remains constant during simulation. This assumption prevents the model from capturing steady-state voltage variations and runtime information. The “impedance-based electrical models” [29], [30] use a complicated equivalent network to fit the impedance frequency spectra in a process that is complex and unintuitive. These models only work for a fixed SoC and temperature setting, thus being unable to predict DC response and runtime. “Runtime-based electrical models” [31], [32], [33] use a complex circuit network to simulate battery runtime and DC response for a constant discharge current in circuit simulators. However, they cannot predict neither runtime nor voltage response for varying loads. A summary of the features of each ECM is presented in Table 1.

Table 1. Comparison of Various Equivalent Cell Models.

Predicting capability	Thevenin-based model	Impedance-based model	Runtime-based model
DC	No	No	Yes
AC	Limited	Yes	No
Transient	Yes	Limited	Limited
Battery runtime	No	No	Yes

Chen and Rincon-Mora presented a widely-used ECM as shown in Figure 2 [22]. This model is capable of predicting both the steady state and transient responses, as well as the battery runtime of Li-ion cells, while also being intuitive and easy to understand. This ECM comprises two separate parts:

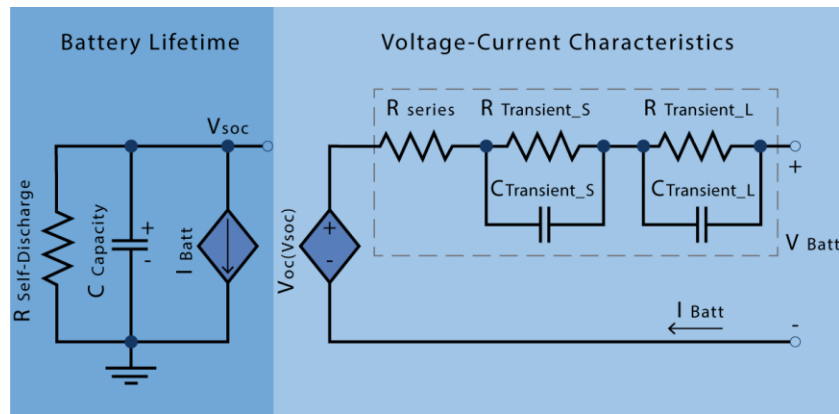


Figure 2. De-coupled ECM by Chen and Rincon-Mora [22].

1. Battery lifetime: Composed of a self-discharge resistance $R_{\text{Self-Discharge}}$, a storage capacitor C_{Capacity} and a controlled current source I_{Batt} , all connected in parallel. The capacitance of the capacitor is assigned in such a way that it correlates to the varying SoC of the cell under the given current of the controlled source. The self-discharge resistance is used to simulate the self-discharge phenomena, which for some cases, such as a constantly used battery, can be ignored. The capacitance may be simply calculated as shown in Eq. 1, where cycling and temperature information is not considered.

$$C_{\text{Capacitor}}(F) = 3600 \cdot \text{Capacity} (Ah) \quad \text{Eq. 1}$$

2. Voltage-Current characteristics: This section includes a controlled voltage source $V_{OC}(V_{SoC})$, whose value depends on SoC, normally implemented using a lookup table. A series resistor R_{Series} is also included to simulate immediate voltage response, while a number of parallel *resistor-capacitor* (RC) connections is included to simulate transient response. The quantity of RC branches can be adjusted based on desired model accuracy and computational limitations.

This model is able to accurately represent steady-state and transient responses, while also predicting battery runtime. It is also easy to understand and characterize it using curve fitting algorithms. As SoC calculation is effectively decoupled from the transient response calculation, then the system has an increased robustness. This scheme can also be initialized at any given SoC by assigning an initial voltage to the storage capacitor $C_{Capacity}$.

Besides simulating the electrical behavior of battery cells, current research has also proposed electro-thermal models. Lin et al. have proposed a lumped-parameter electro-thermal model presented in [23]. This model divides a cylindrical cell into two sections, the core and the surface, assigning a temperature value to each one. The system is able to calculate the temperature of both sections by considering the current and voltage of the cell, as well as the ambient temperature. The relationship between the inner and outer temperature is modeled by a series of first-order equations, which can be parameterized to fit experimental data.

2.5.2 Battery balancing background

Battery packs are comprised of arrays of dozens or even hundreds of individual cells. These battery packs contain a mixture of series and parallel connected cells. Lithium-ion cells operate in a voltage range between 1.5 V (low charge) and 4.5 V (max charge) depending on their cathode chemistry [34], [1]. Since individual cells operate with low voltages, as compared to the voltage requirements of modern electrical systems, then series connection is often used to elevate the voltage of the pack as required, while parallel connections are used to increase the current flow through the battery pack. Although parallel-connected cells tend to naturally balance over time, series-connected cell do not have a natural mechanism to balance themselves [18].

The differences between each individual cell in a battery pack can bring down the performance of electric systems, such as electric or hybrid vehicles, and shorten its expected service life. A degraded or aged cell will limit the pack's performance as this cell has lost its ability to provide the expected energy to the system in contrast to healthier cells [10]. To mitigate the effects of these differences, several battery balancing methods have been developed in the literature during the last years. Balancing and equalizing the battery cells, i.e., evening the level of charge in battery cells, can be achieved through several techniques that are often classified in two overall categories: passive and active [12], [14], [15], [16]. These methods comprise several different techniques outlined in Figure 3, and described in the following subsections. It is important to note that many of these individual methods can be combined to further enhance the battery balancing system capabilities.

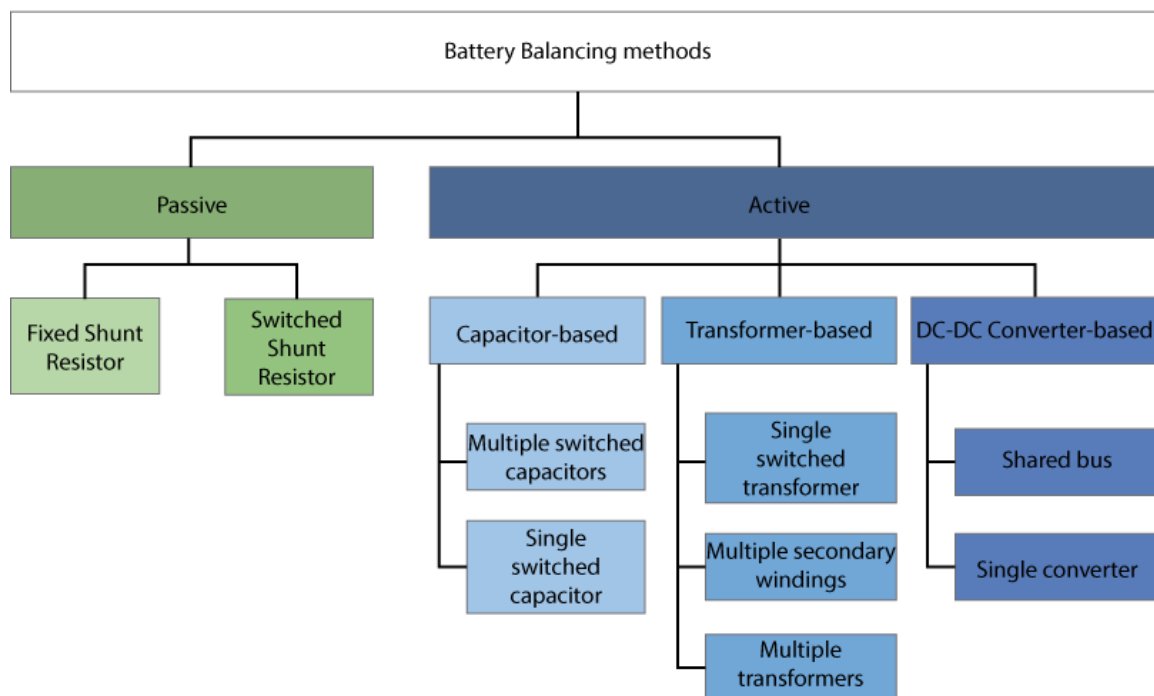


Figure 3. Classification of active and passive battery balancing and equalization methodologies [18], [12], [15].

2.5.3 Passive balancing methods

Passive balancing removes charge from cells that have a higher SoC than others and dissipates the drained energy as heat, which is often achieved by dissipating the excess charge through a number of resistors matching the number of individual cells in the pack. In these designs, a resistor is connected in parallel to each cell to drain energy from it. The advantages of the passive methods are the low cost of the circuitry and the facility of implementation, compared to more complex active methods [5]. Nonetheless, the extra energy is dissipated as heat, which can increase the pack temperature, driving up the requirements for cooling and limiting the overall performance of the battery. Passive methods can be further classified depending on how the dissipative resistor is connected to the battery cell. Due to their simplicity and low cost, these methods are still implemented in battery packs as shown by Perișoară et al. [7] and Amin et al. [8]. However, other authors have reported that this approach is limited to charging cycles, as there may be a waste of energy during discharge [12].

2.5.3.1 Fixed shunt resistor

In this topology, the dissipative resistors are permanently connected to their respective cell. The general ideal behind this method is that cells with higher SoCs will have a greater balancing current, and thus self-discharging faster than cells with lower SoCs. This circuit is constantly dissipating charge, even at times when the pack is already balanced. An alternative to this problem is the usage of Zener diodes to stop the current flow through a cell when its voltage drops below some point, i.e., the nominal voltage of the diode. When the cell voltage is above the Zener setpoint, the resistor path is activated, depleting the cell's charge until the cell's voltage is lower than the setpoint [18]. However, this design works for battery chemistries that allow some level of overcharge, such as lead-acid, but not for Li-ion batteries. Figure 4 shows the typical configuration for fixed shunt resistors, as well as the modified version including Zener diodes for discharge control.

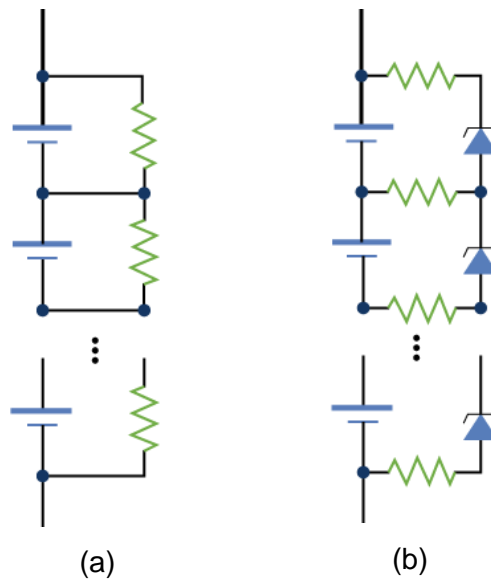


Figure 4. Typical fixed shunt Resistors topology (a) and Modified Zener-fixed shunt resistors topology (b) [18].

2.5.3.2 Switched shunt resistor

In this topology, the direct connection between the cell and the resistor is replaced by a switch that is controlled by an algorithm, allowing for greater flexibility in the balancing strategy. Different control schemes can be accommodated under this circuitry. The simplest method consists of turning on all switches during charging, as more current will go through the resistor connected to the highest voltage cell. In contrast, a more complex algorithm may involve voltage sensing to determine which cells must dissipate excess of energy [12]. These switches are normally built with high-current transistor circuits. This configuration is shown in Figure 5, where generic symbols are used to represent the control unit and the switches. This technique has been widely explored in both industry and research, where some authors have reported an energy efficiency of up to 94% under lab conditions [9].

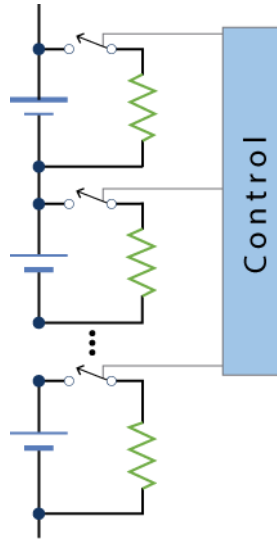


Figure 5. Switched shunt resistor topology [12].

2.5.4 Active balancing methods

Active balancing methods remove charge through an intermediate bridge (physical component through which charge can be moved) that absorbs charge from fuller cells to deliver it to emptier cells, conserving the overall energy in the battery pack [12]. These methods represent a promising possibility to enhance energy efficiency, since energy is not dissipated on purpose, although at the expense of a higher circuitry complexity, which can potentially elevate the costs of the balancing system [13]. As the active balancing methods support degraded or aged cells among other cells, these techniques can bring the battery pack to a uniform end of life condition [18]. As moving charge between cells instead of dissipating energy is more efficient, these techniques can be usually applied during both charge and discharge. Different components can be used to move charge between cells; the following subsections explain them in detail.

2.5.4.1 Capacitor-based balancing methods

These methods use capacitors as a bridge to redistribute charge across cells. The most basic capacitor balancing circuit consists of a series of capacitors connected to the battery cells through single-pole-double-throw switches that repeatedly shift back and forth [15]. The objective of this technique is to synchronize the voltages of two adjacent cells by connecting a common capacitor in parallel alternatively [12]. Generally, there is one fewer capacitor than individual cells, as each capacitor is connected to the high side

of one cell and the low side of the next one, as shown in Figure 6. Through the shift of the switches, the high-voltage cell charges the capacitor up to reach its same voltage, and then, the low-voltage cell discharges the capacitor to its same voltage, moving the charge from one cell to its neighbor. Nevertheless, this method can take a long time before the whole pack is balanced, as charge must travel from the fuller cells to the emptier cells, passing through all the cells between them. All of the switches can be generally controlled by the same control signal, with a fix duty cycle of 45% for each switch position [12]. This method avoids closed loop and SoC calculation, as the cells are automatically balanced. Figure 6 shows an example of this configuration, where a generic *electronic control unit* (ECU) controls the switches that connect the cells to the capacitors. It is important to note that these switches are often implemented using transistor circuits, in particular MOSFETs.

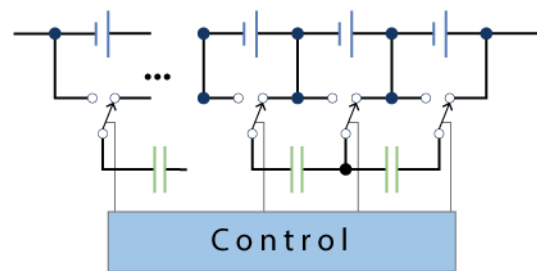


Figure 6. Typical switched capacitors topology [15].

To speed up the balancing process, Qi and Dah-Chuan Lu have proposed topologies in which additional capacitors are added to the design [12]. Figure 7 (a) shows that an extra tier of capacitor provides additional paths for charge transferring, i.e., cells that are not adjacent can transfer charge through the added capacitors. In this way, non-adjacent cells can move charge between them, achieving shorter balancing times. Figure 7 (b) shows another alternative design by connecting a single additional capacitor between the last and the first cells of the module, forming a closed loop. Through this capacitor, a high quantity of cells can be bypassed, as charge can flow through the shortest path.

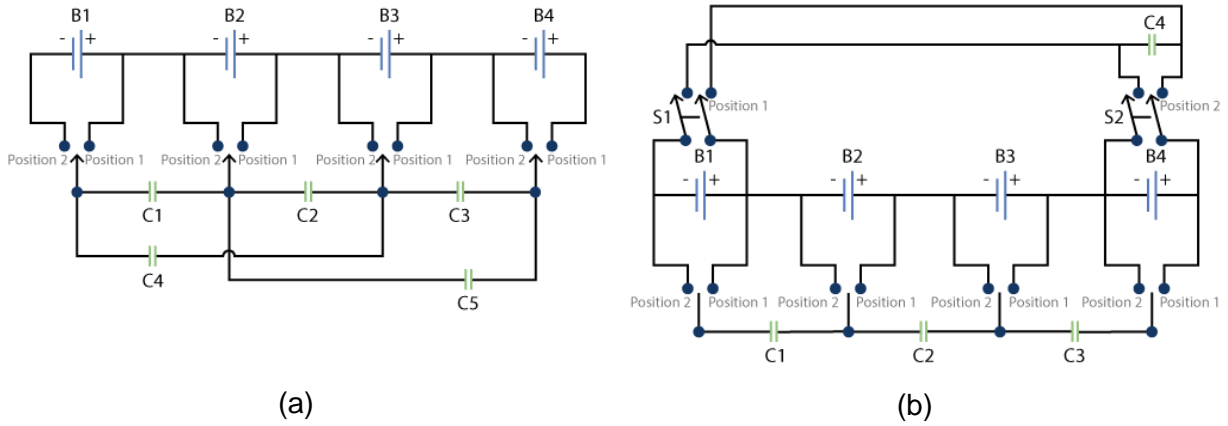


Figure 7. Switched capacitors with double tier topology (a) and Circle patch switched capacitors topology (b) [12].

An alternative to the previous designs is to use a single capacitor (also known as flying capacitor) connected to the battery pack through switches controlled by an algorithm running on an ECU [15]. This topology allows direct movement of charge from one highly charged cell to a lowly charged one. With this control scheme, the cell with the highest SoC is connected to the capacitor to charge it up to the cell's voltage. Next, the capacitor is connected to the cell with the lowest SoC, providing it with charge. This process is repeated until all cells are equalized. Figure 8 shows a topology where an ECU decides which cell must be connected to the capacitor by controlling each switch. Although this method can balance cells in a shorter time, a large number of switches is required, which causes some energy dissipation as heat in both the switches and the capacitor. Additionally, it must be noted that this method requires voltage sensing and SoC calculation, as the balancing process is not natural. A control strategy must be developed to determine the order in which the cells must be connected to the capacitor.

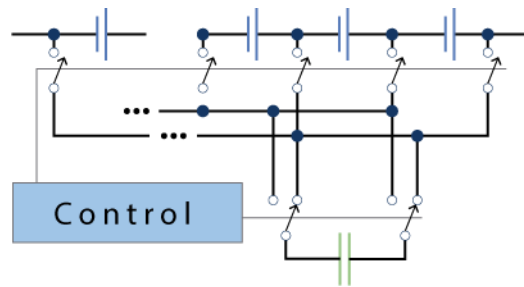


Figure 8. Single switched capacitor topology [15].

These methods are not convenient for Li-ion cells as most cells experiment very little voltage variation between them, even when their SoCs may differ greatly, and as capacitor topologies rely on voltage differences between cells in order to work, these methods may result in long balancing times [18]. Moreover, aged cells can also degrade the effectiveness of balancing through capacitors due to the variation in capacities among the cells, which may lead to voltage balancing issues [12]. It is worth noting, that although the methods presented in this section are more energy efficient than the passive techniques, some energy is still lost as heat due to the parasitic resistance of the switches. These losses are smaller than in passive methods, but are larger than the losses experienced by other topologies such as transformer-based balancing circuits [15].

2.5.4.2 Transformers-based balancing methods

In these methods, transformers are used as the bridge to redistribute charge between cells. Transformers convert AC electrical energy from one voltage range to another, e.g. from 120 V to 12 V, depending on the relation between the number of turns in primary and secondary windings. This idea has been explored to quickly move charge from one cell to another with minimal losses [15]. Although battery cells and packs operate at DC, rapidly shifting a switch connected to the primary side of the transformer can approximately create an AC signal, which is then transferred to the secondary winding and rectified to be fed to a particular cell [18].

In the basic topology based on transformers for active balancing, a single transformer is used to move charge between cells. The primary of the transformer is connected across n cells, with the secondary connected to each cell through a halfwave rectifier and several electronically controlled switches. With this design, charge from the overall battery pack is redistributed to the cells with lower SoCs, faster than in capacitor-based designs, although at higher costs due to the transformer complex magnetic design itself, as well as its higher parts count [15]. Figure 9 shows this topology, where an ECU determines which cell must be connected to the rectified signal in the secondary winding, while approximating an AC signal through the rapid shifting of a single switch.

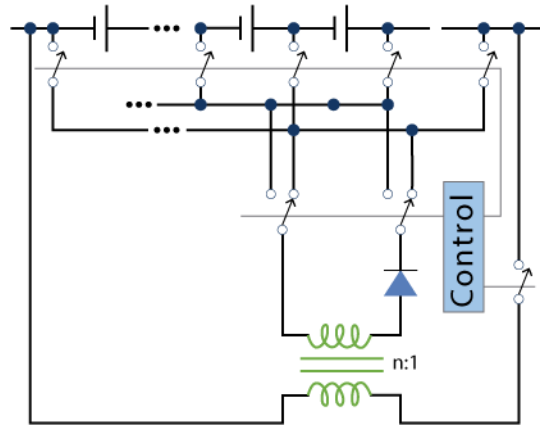


Figure 9. Basic transformer topology [15].

Some authors show an alternative to the previous design, where a transformer with a secondary winding per each individual cell is used [34], [12], [15]. The AC signal is still generated by a single switch connected to the primary side of the transformer, but now all the cells are connected to a secondary winding that provides current to low-voltage cells. This topology does not require sophisticated control algorithms, although a transformer design tailored to the specific needs of the battery module is required. Nevertheless, such consideration could be expensive or impractical. Since the cells are permanently connected to the secondary windings, rectifier diodes must be added to the circuit to ensure the adequate direction of current. Figure 10 (a) shows an example of this configuration, in which an ECU is required to produce the AC signal.

Qi and Dah-Chuan Lu have also provided a method that avoids the need of a custom transformer by using multiple simple transformers [12]. In this topology, each cell is connected to an individual transformer. The primary windings of the transformers are connected in parallel to each other and to the terminals of the battery pack. The secondaries are then connected to each of the cells. With this arrangement, the charge is distributed directly from the battery pack to the cells with less charge. A diode to rectify the current flow must also be included in this configuration as there is no means to disconnect the cells from the transformers. Figure 10 (b) shows this topology, where an ECU controlling the shifting of switch S1 to generate the AC signal is included. A more complex configuration has been proposed by Ran et al., where opto-electronic switches are used instead of an array of transistors [3]. Ouyang et al. have proposed a topology

that combines the transformer and capacitor-based designs, resulting in a module with low heating, low energy consumption, and short balancing time [17].

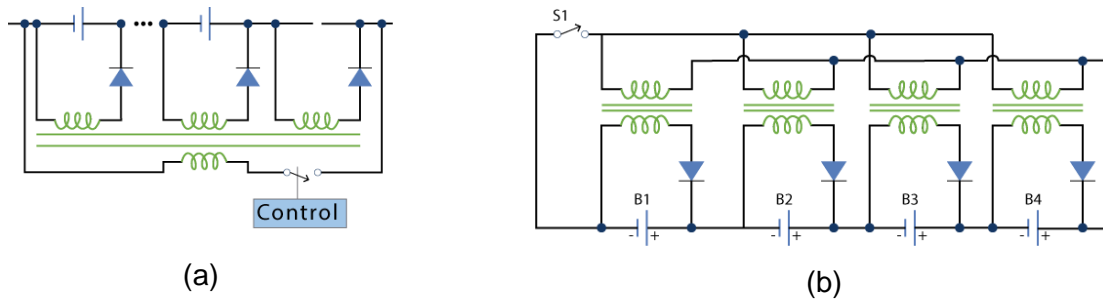


Figure 10. Multiple secondary windings topology [15] (a) and Multiple simple transformers topology [12] (b).

2.5.4.3 DC-DC converters-based balancing methods

In recent years, Plett [18], Pham et al. [5], and Qi and Dah-Chuan Lu [12] have presented new designs for active balancing that utilize small bidirectional DC-DC converters to connect the cells to a shared capacitive low-voltage bus, which performs the balancing. One of these designs uses a converter to connect each cell to the shared low-voltage bus. A custom “balancing metric”, which can be different than simply SoC or cell voltage, is mapped to a DC level (normally between 9 V and 14 V). If the cell metric is above the shared bus voltage, the cell must provide charge to the shared bus; otherwise, the shared bus should charge the cell, instead. Figure 11 (a) shows the basic multiple DC-DC converter circuit design, while Figure 11 (b) shows an example of a bidirectional converter.

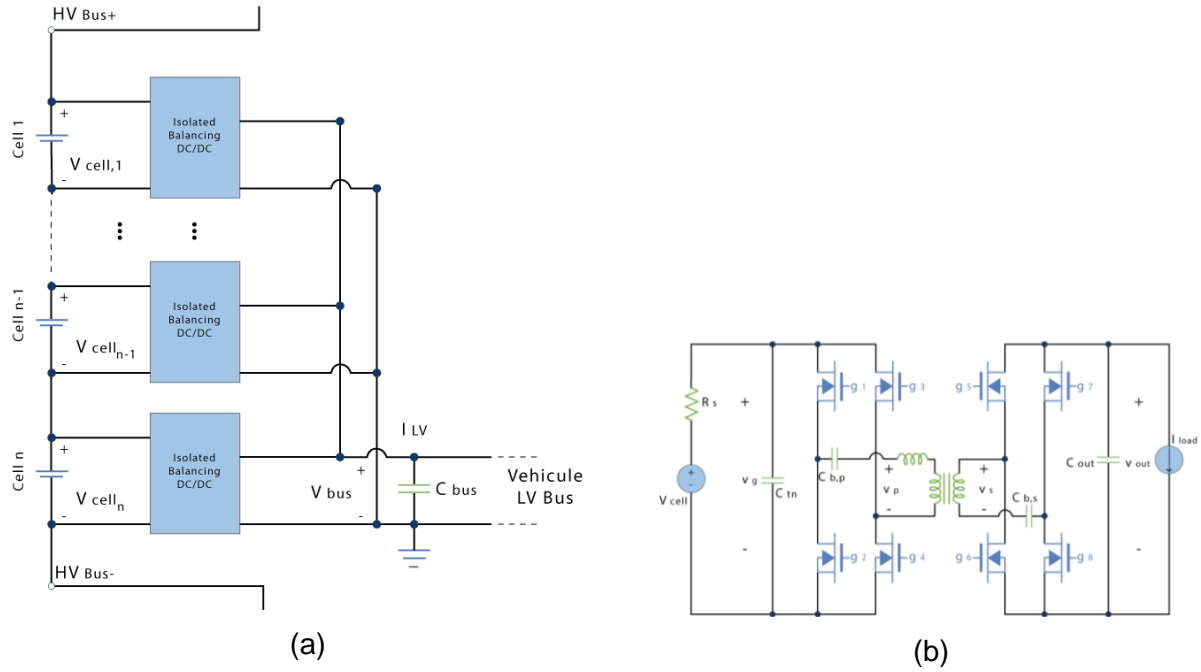


Figure 11. (a) Shared low voltage bus topology, and (b) example of a dual-active-bridge DC-DC converter circuit [18].

The low-voltage bus in this design can even provide power to auxiliary loads. If the load power is large and consistent enough, the bidirectional converters can be replaced with unidirectional converters, lowering the cost of the design. This topology can also be equivalent in cost when compared to passive methods since the overall pack cooling needs are reduced and the shared bus can even replace costly large DC-DC that converters normally used to convert pack voltage to 12 V for vehicle auxiliary loads.

Park et al. have proposed a similar design, where instead of using a capacitive shared bus, a transformer with multiple secondary windings is implemented [4]. The primary side of transformer is connected in parallel to the battery pack, while each secondary winding is connected to a DC-DC converter, which is then connected to a single cell itself. High balancing speeds have been achieved with this configuration, as parasitic resistances have been eliminated. This topology is shown in Figure 12 where the transformer-based bus and the basic design of the converters can be observed.

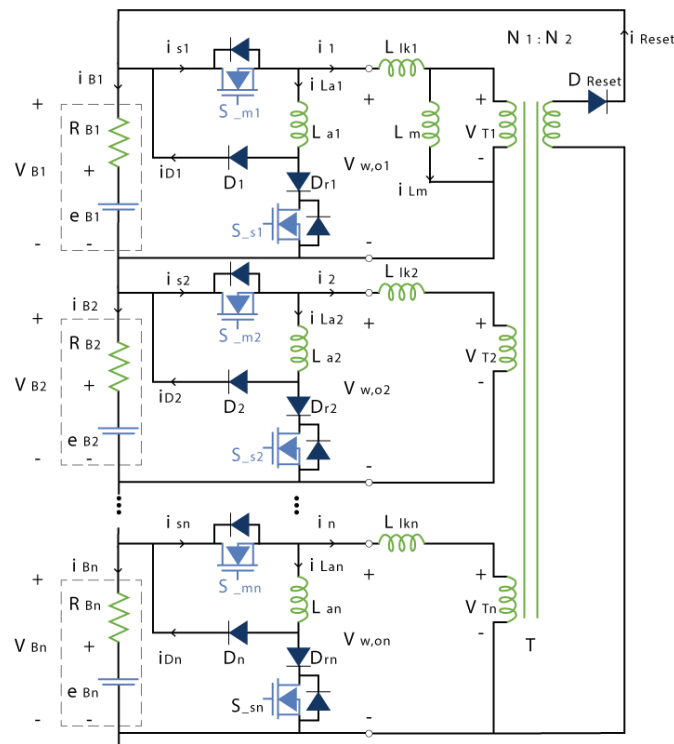


Figure 12. Multiple DC-DC converter topology with transformer-based bus [4].

Huang and Abu Qahouq have presented an alternative to the multiple converters design, where each battery cell is only connected to a bidirectional DC-DC converter and not to the other cells [35]. The converters are then connected in series to each other to obtain the required voltage of the battery pack. Each converter can provide charge from the pack to each cell to balance it. With this approach, there is no need for two independent converter systems for cell balancing and DC bus voltage regulation.

A different approach to the one presented by Qi and Dah-Chuan Lu, consists in the use of a single DC-DC unidirectional converter connected to the battery pack on one side, and to each individual cell on the other side [12]. The connections to the individual cells are done via electronically controlled switches. With this design, charge from the whole pack can be distributed to a single cell with a low SoC. An example of this configuration can be seen in Figure 13, where every switch (s1-s4) must be controlled by an ECU determining which cell needs to be balanced by the DC-DC converter.

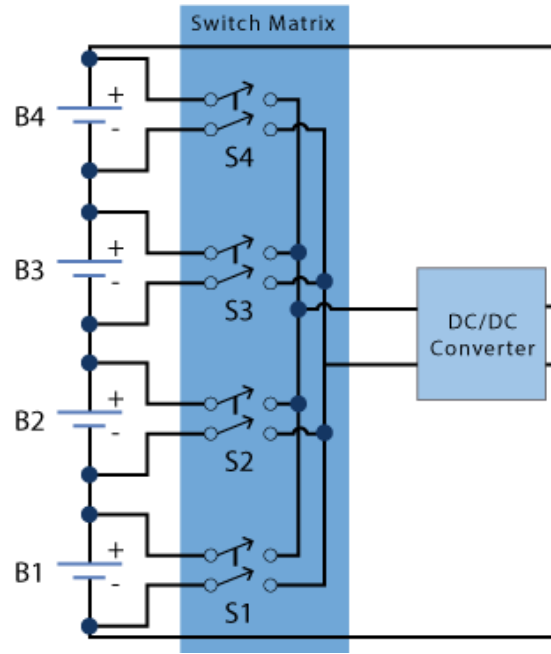


Figure 13. Switch matrix topology with a balancing DC-DC converter [12].

Recently, several authors have continued researching active cell balancing methods based on DC-DC converters of varying complexity with the goal of reducing cost and achieving higher efficiencies. Zun et al. have proposed a balancing topology that uses DC-DC converters to isolate cells during charging. Each converter sets the reference value for each individual cell, and only the cells that do not achieve the reference value receive additional charge, which reduces the mutual influence between the cells, reducing losses and shortening the balancing time [36]. In similar way, Wu et al. have developed a topology that is able to inject additional charge to specific cells based on their current SoC during charging [37].

2.5.5 Balancing algorithms

A balancing algorithm is a computational routine that can identify which cells require balancing, either by sending excess energy in one of the cells to the battery pack or by feeding additional charge to one of the cells from the available energy in the battery pack. Zheng et al. have identified that current literature presents two common methods [14]. The first one consists on evaluating each cell's voltage. When the difference of one of them compared to the mean cell voltage is above certain threshold, then the cell is

selected as a candidate for balancing. While this represents a simple algorithm to be implemented, the external voltage of a cell depends on its internal states and environment [21], that is, the cell voltage itself may not represent accurately its SoC.

The second type of algorithms is based on the SoC. These methods calculate the remaining stored energy of the cells and, when one of them is different from the others outside certain limits, the cell is selected for a balancing operation. Nevertheless, since SoC cannot be measured directly, these methods are affected by inaccuracies in the battery model, as well as influenced by self-discharge, temperature, and other factors [21].

Piao et al. have proposed an outlier detection methodology, which is a technique used heavily in data mining [21]. With this algorithm, several cell parameters and variables can be observed at the same time to identify overcharged or undercharged cells, i.e., those showing different behavior when compared to other cells with a normal performance. This method can be configured to consider certain variables (terminal voltage, temperature, SoC, SoH, among others) to calculate a statistic distance from one cell to another, which serves to identify outlier cells. Further exploring this algorithm could result in a more flexible technique for cell selection that could handle diverse operation conditions and varying grades of uncertainty with better results than simpler methods existing today. Furthermore, Yang et al. have developed a balancing algorithm based on graph theory, which is mainly intended for balancing *energy storage systems* (ESS) under a *distributed generation* (DG) scheme [38].

2.5.6 Summary and trends

As remarked in this section, passive balancing methods dissipate excess energy from cells having higher SoC, while active balancing topologies redistribute excess energy from highly charged cells to cells with lower SoC.

The impact of balancing circuits on battery health has also been studied. A long-term test including a post-mortem analysis of the individual cells has been carried out by Ziegler et al. [16]. This study shows a capacity increase of 2%, as well as a reduced deviation in capacity and internal resistance on battery packs that have been actively

balanced as compared to those balanced using passive methods. Zheng et al. have also reported a counterproductive result in battery pack capacity when using passive balancing methods during discharge [14].

It is worth noting that there is a lack of a systematic and comprehensive comparison between balancing circuits in the literature [14]. As balancing systems are tested on particular battery packs specified by the authors of each methodology, results from consistent battery packs need to be evaluated and compared. To summarize the findings of this review, Table 2 shows the advantages and disadvantages of the methods presented in this section.

Table 2. Summary of advantages and disadvantages of balancing methods

Balancing	Method	Advantages	Disadvantages
Passive	Fixed shunt resistors	Low complexity Low cost No ECU required	Wastes energy, even when the pack is balanced Generates additional heat
	Switched shunt resistors	Low complexity Low cost	Wastes energy Generates additional heat ECU required Long balancing time
Active	Multiple switched capacitors	Low complexity Low cost Less generated heat Less wasted energy	Long balancing times ECU required Relies on voltage differences
	Single switched capacitors	Low complexity Low cost Minimum generated heat Minimum wasted energy	ECU required Relies on voltage differences

		Faster balancing time than passive methods	
	Single switched transformer	Fast balancing time Minimum generated heat Minimum wasted energy	High costs of transformer High space claim ECU required Complex switching algorithm
	Multiple secondary windings	Fast balancing time Minimum generated heat Minimum wasted energy No complex switching algorithm	Higher costs of custom transformer High space claim ECU required
	Multiple transformers	Fast balancing time Minimum generated heat Minimum wasted energy No complex switching algorithm	Higher costs due to transformers High space claim ECU required
	DC-DC converter (Shared bus)	Fast balancing time Minimum generated heat Minimum wasted energy Can power auxiliary loads Can replace large converters	Higher costs due to DC-DC converters High complexity ECU required
	Single DC-DC converter (Switch matrix)	Fast balancing time Minimum generated heat	High cost due to larger DC-DC converter Medium complexity

		Minimum energy	wasted	ECU required
--	--	-------------------	--------	--------------

Furthermore, balancing methods can be combined with each other as shown by Lin et al. [39]. In this work, the authors present a design for two battery modules where the individual cells are balanced through a passive balancing system when charging. In addition, during online operation, a DC-DC converter is activated to balance one module with respect to the other, minimizing energy loss.

Recent investigations also show how different active cell balancing methods can be combined to produce faster balancing times and improve energy efficiency. Han et al. have proposed a topology where a multi-winding transformed is combined with a buck-boost converter to achieve direct cell-to-cell balance achieving high balancing efficiency and speed, specifically, for circuits with low voltage and high current [40]. Furthermore, Pham et al. have developed a balancing topology that combines a push-pull converter, a single transformer, and an array of relays to achieve cell-to-cell balance [5]. This circuit is able to reach high balancing speed and efficiency, while also keeping implementation costs lower as no expensive gate driver circuits are used [5].

Latest researches, such as the work by Vardhan et al. [41], Moghaddam and Van den Bossche [42], and Narayanaswamy et al. [43] have introduced the idea of using inductors coupled with other DC-DC converters to build active balancing topologies. These new circuits tend to target cell-to-cell balancing, although some of them can be configured to cover multiple balancing schemes. Nevertheless, they still carry high implementation costs due to their complexity and additional required components and more involved control methods.

2.5.7 Remarks on current technologies

The author of this work has found that even though passive balancing is simple, there is still some development in this field as it can be an adequate method during charging cycles. Nonetheless, as these methods dissipate energy, they are not suitable as a balancing method during online operation. Therefore, lower energy efficiency is

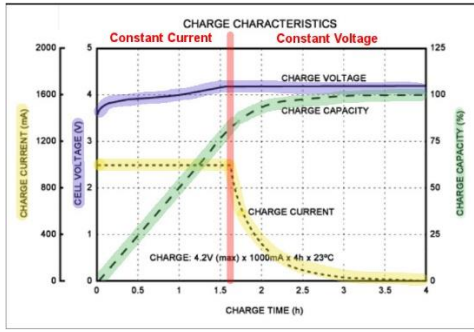
achieved by passive balancing. In contrast, active balancing methods might be better suited for online applications where charge and discharge cycles can happen randomly, e.g. when driving an electric vehicle.

Considerable research has been done in designs involving DC-DC converters during the last years, as their high efficiency and fast balancing times make them very attractive for the EV market. Since the costs associated with this kind of designs are still high, a novel design targeting modularity and lower implementation costs could prompt companies to start using active balancing in their BMS designs. As most industrial applications continue to apply passive balancing, there exists a good opportunity area to change the paradigm [20].

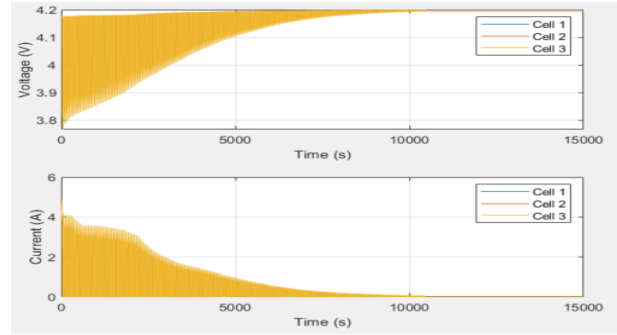
Moreover, significant improvement can also be obtained by developing novel balancing algorithms. As conventional algorithms are based on a single variable at a time, they may be prone to inaccuracies derived from external cell factors and imprecisions in the cell model [21]. Therefore, by considering multiple factors, excessive cell stress due to inconsistencies in the balancing algorithm can be avoided, improving the performance of the balancing system, and keeping a low impact on battery pack service life.

2.5.8 Charging profiles

Li-ion cells are normally charged using a *constant current constant voltage* (CCCV) charging profile. Any BMS should be able to implement this charging method, while ensuring that cells are kept within their operational limits. Other charging schemes have also been proposed in the literature following non-conventional ideas. One of them, the *pulsed constant voltage* (PCV), results of interest to this research work as it targets both a fast charge with less temperature raise. These two profiles are explained in the following sections. Figure 14. (a) CCCV charging profile, and (b) PCV charging profile.



(a)



(b)

Figure 14. (a) CCCV charging profile, and (b) PCV charging profile

2.5.8.1 CCCV charging profile

The CCCV scheme consists of a constant current control stage followed by a constant voltage control stage. The system switches between the two stages once a threshold battery pack voltage has been reached. The CCCV scheme works as follows:

1. CC: While the battery pack voltage is below the threshold of the transition switch, the current source is connected to the battery pack, providing a steady current at a given C rate.
2. CV: Once the battery pack voltage reaches the threshold voltage, a constant voltage is then applied to the battery pack, until current is below 1/10 of C rate.

It is worth noting that this charging scheme is one of the most commonly used in today's applications. Therefore, any balancing system must ensure correct operation during the CCCV charging cycle.

2.5.8.2 PCV charging profile

This method consists in exposing the battery pack to pulses at a constant voltage (the top charging voltage), while adjusting the duty cycle to achieve a balance between charging time and temperature rise. A duty cycle of 50% is generally used as it provides this balance; however, the authors in [44] have also proposed a method in which they inject these CV pulses at different duty cycles and evaluate the response of the battery pack to determine the ideal duty cycle for a portion of the charging period.

2.6 System description – Case study

Data from 18650 Li-ion battery cells with a nominal capacity of 2 Ah was obtained from the datasets presented by Bole et al. [45]. This data describes the behavior of a group of cells under different “random walk” discharging experiments.

A “random walk” discharge test consists on using a randomized sequence of discharging current between 0.5 A and 4 A. The different datasets belong to tests in which the discharge rates were skewed to higher or lower currents, as well as run at different temperatures. After every fifty “random walk” cycles, a series of reference charging and discharging cycles were performed to provide insights about the battery *state of health* (SoH).

The data that was used to characterize the cells was obtained from the set named “room temperature random walk discharging data sets”. In this dataset, four cells were charged to 4.2 V and then discharged to 3.2 V using a uniformly distributed set of discharging currents between 0.5 A and 4 A at room temperature.

Modelling and simulations will be focused on modules of no more than 20 cells connected in series. Parallel connections are not considered here as they ensure balance and equalization naturally. However, it is important to make sure that the individual cells connected in series inside each of the modules are balanced and equalized to maximize performance and battery life.

2.6.1 Mathematical model of Li-ion battery cell

The mathematical model chosen for the basis of battery pack simulation is the ECM proposed by Chen and Rincón-Mora due to its ability of accurately representing steady-state and transient responses, while also allows prediction of the battery runtime [22]. The structure of this model is shown in Figure 15.

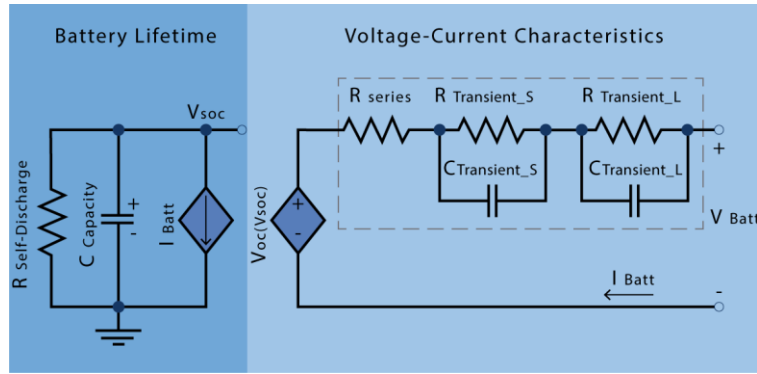


Figure 15. ECM selected for simulation purposes [22].

The parameters for this model have been estimated with the information obtained from the *random walk* (RW) datasets and the process described in Appendix I. Only one RC branch has been implemented, as validation experiments with the available data confirmed that this specific model exhibited enough accuracy, as compared to two and three branches models. Table 3 summarizes the parameters for the tuned model.

Table 3. Cell parameters of the 1RC cell model after parameter estimation.

SoC	VOC (V)	R_0 (Ω)	R_1 (Ω)	C_1 (F)
0	3.6888	0.1002	0.0153	80.0089
0.0909	3.7390	0.0840	0.0148	83.3790
0.1818	3.7671	0.0889	0.0144	84.8834
0.2727	3.7842	0.0879	0.0149	72.1798
0.3636	3.8043	0.0827	0.0147	75.6232
0.4545	3.8318	0.0923	0.0145	78.1657
0.5455	3.8836	0.0836	0.0144	79.3352
0.6364	3.9337	0.0886	0.0151	74.9573
0.7273	3.9888	0.0896	0.0142	74.0637
0.8182	4.0475	0.0875	0.0143	73.7476
0.9091	4.1172	0.0853	0.0134	79.1092
1.0000	4.1976	0.0923	0.0083	134.1446

2.6.2 Construction of battery pack

The data extracted from the RW discharging experiments has been used to build a module comprised of 20 cells connected in series. The nominal voltage of each cell is 3.6 V, which provides a nominal voltage of 72 V for the overall module. The maximum charging voltage per cell is 4.2 V, which corresponds to a maximum of 84 V for the whole pack.

A building block comprising an individual cell has been created as an element in a Simulink™ library. Twenty instances of this block have been created and connected in series to represent the cells in the battery pack. Auxiliary blocks for measurements and control have also been created. Figure 16 shows the individual cell block and a portion of the battery pack comprising these elements, where T1 (+) is the positive terminal of the cell, T2 (-) is the negative terminal, H is the thermal connection, Sensor_Bus represents a bus containing temperature, SoC and terminal voltage, VT_Cell is the terminal voltage of the cell, I_Cell is the current flowing through the cell, and SOE_Cell is the state of energy (SoE) of the cell. To create a battery module, the T1 (-) terminal of one cell is connected to the T1 (+) terminal of the next cell. The T1 (+) terminal of the first cell must be connected to the positive terminal of the power supply or load, while the T1 (-) terminal of the last cell in the module must be connected to the electronic ground reference. The Sensor_Bus and other state information out of a “Single_Cell” block must be connected to a single “Sensor Block” for further processing.

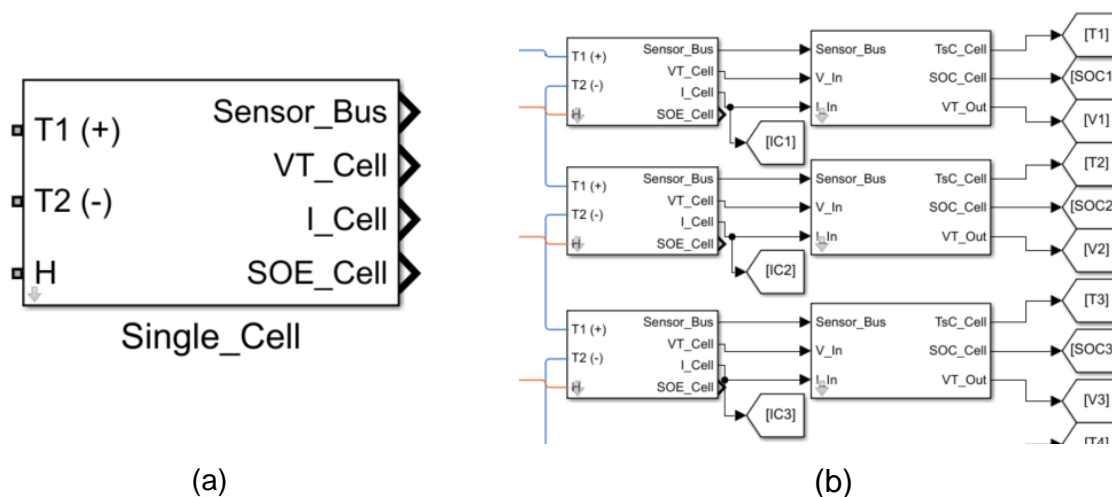


Figure 16. (a) Individual cell block and, (b) portion of battery pack comprised of individual cells and sensor blocks.

Chapter 3

Development

This section explains the development of the proposed balancing system, focusing on the specifications of the balancing algorithm and topology.

3.1 Proposed balancing system overview

In this section, a general overview of the proposed balancing system is presented. The following sections present the details of both the developed balancing topology and the proposed algorithm.

The proposed balancing system is composed of an active topology with a DC-DC converter based on the structure developed by Murshadul et al. [46]. The structure is then coupled to a multi-factor cell selection algorithm following similar ideas as in the work of Piao et al. [21], and using a newly-defined control strategy based on cell SoP. The active topology, control strategy and selection algorithm work together to provide fast balancing results, while ensuring that cells are safely operated. Figure 17 shows the elements of the proposed balancing system.

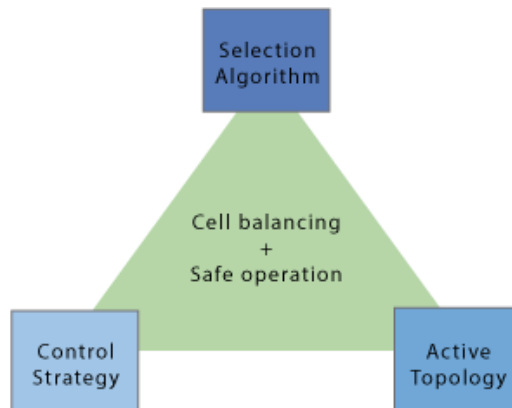


Figure 17. Elements of the proposed balancing system.

3.2 Development of the balancing topology

This segment explains the proposed active balancing topology, including the details of the DC-DC converters.

3.2.1 Proposed balancing topology

Since energy is not being intentionally dissipated during an active balancing, the energetic efficiency is expected to be higher than in a passive balancing scheme. Under the premise of a higher energetic efficiency, an active balancing topology based on the implementation of DC-DC converters has been developed. The active balancing topology proposed in this work consists of two DC-DC converters that can be connected in parallel to each individual cell through an interface, referred to as the switch matrix. This idea is based on the topology proposed by Murshadul et al. [46].

A first DC-DC converter takes energy from the battery module and injects an extra balancing current to a given cell, as determined by the balancing algorithm. This means that this specific converter receives the module voltage as the input and delivers the required cell voltage to achieve the desired balancing current. For convenience, this converter will be referred to as the “charging converter”.

A second DC-DC converter is aimed to extract current from a given cell and re-inject it into the battery module. This converter receives the current of the cell to be discharged at a low voltage and delivers a current at a higher voltage, close to the voltage of the battery module. This converter is referenced as the “discharging converter”.

A change in the output of any DC-DC converter generates an immediate response in the battery cell, evidenced by a sudden change in the cell current. This is due to the fact the battery cells are modeled as a controlled-voltage source coupled with a series resistor and an RC branch. To soften the dynamics of the cell’s current response, an LC filter is added at the end of each DC-DC converter. This filter smooths the changes in the current, allowing for the introduction of a proper controller for the cell current.

Figure 18 represents a small subsection of the proposed balancing circuit, showing only three Li-ion cells and their corresponding switches. Each DC-DC converter is connected to an LC filter. Every battery cell is connected to the output of the LC filters through a *double-pole single-throw* (DPST) switch. This switch enables the parallel connection of each Li-ion cell to the DC-DC converters. The discharging and charging converters are connected to the complete battery pack to redistribute energy from and to the cells. On the one hand, the balancing current I_{bal} flows from a cell of the battery module and through the switch matrix when the discharging converter is activated. On the other

hand, I_{bal} is injected to a cell of the battery module when the charging converter is activated instead.

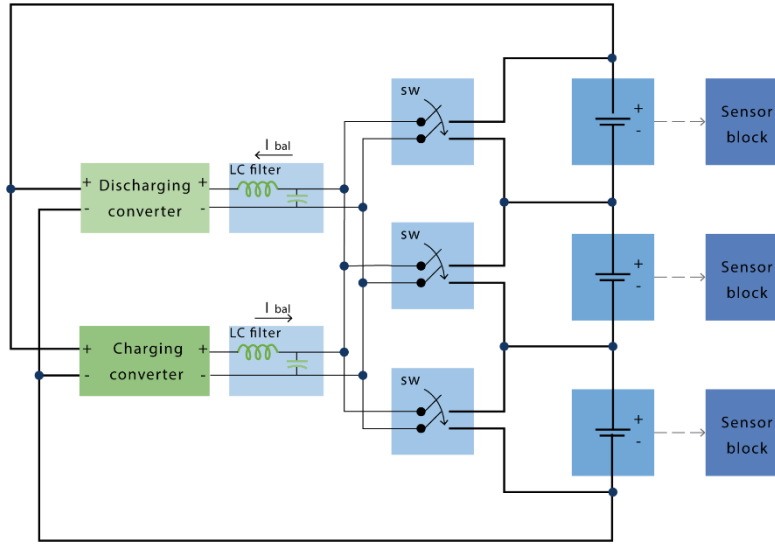


Figure 18. Basic layout of the proposed active balancing topology.

3.2.2 Design of DC-DC converters

The two converters have been designed and implemented as isolated Flyback DC-DC converters. With this configuration, the converter can be connected in parallel to any single cell without causing any disruption or short circuit, with guaranteed isolation between the input and output. This design is also characterized for its low power consumption and a low quantity of parts [47]. Furthermore, Flyback converters have been widely adopted to provide regulated output voltages for low-power applications, typically ranging from 20 to 200 W [48]. Each Li-ion cell has a voltage range of 2.6 V to 4.2 V and a current output of up to 10 A, providing up to 42 W. Therefore, the power range of the Flyback converter covers the power that each cell can inject or receive.

These converters were implemented as Simulink™ blocks, instead of SimScape™ blocks to speed up the simulation. The design of the DC-DC converters was based on the guidelines presented by Hart [49], while the Simulink™ implementation was based on the work by Raj et al. [50]. Figure 19 shows the schematic for the design of the Flyback DC-DC converters.

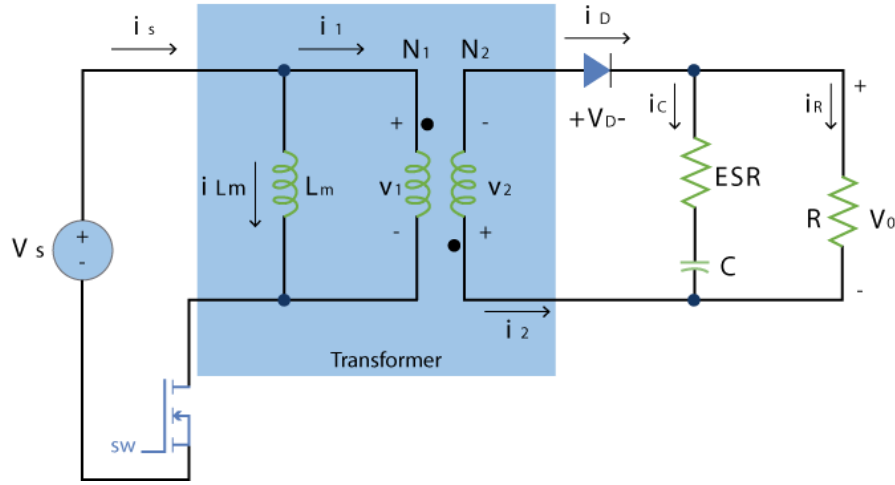


Figure 19. Flyback DC-DC converter schematic.

The parameters which are common to both converters are shown in Table 4:

Table 4. Common parameters for the two DC-DC converters.

Parameter	Description	Value
f_{sw}	Switching frequency	100 kHz
ESR	Capacitor resistance	1 $\mu\Omega$
$R_{DS,ON}$	Switch resistance	1 m Ω
Vd	Diode forward voltage	0.7 V

For the design of the charging converter, an arbitrary turn ratio (N) of 3 was selected. Then, a nominal Duty Cycle (D_{nom}) was calculated using the output voltage equation as shown in Eq. 2, where the minimum module voltage is used as the voltage input (V_s) and the max cell voltage as the output voltage (V_o). Next, the required minimum mutual inductance (L_{mMin}) value was calculated through Eq. 3. However, a higher value of mutual inductance L_m was chosen to guarantee that the converter always operates in continuous conduction mode.

$$V_o = V_s \left(\frac{D_{nom}}{1 - D_{nom}} \right) \left(\frac{N_1}{N_2} \right) \quad D_{nom} = 0.1461 \quad \text{Eq. 2}$$

$$L_{mMin} = \frac{(1 - D_{nom})^2 R \left(\frac{N_1}{N_2} \right)^2}{2f} = 164 \mu H \quad \text{Eq. 3}$$

$$L_m \geq L_{mMin} \quad \text{Eq. 4}$$

A voltage ripple of 0.15% was selected to ensure proper output voltage response. The capacitor value (C) required for this output was calculated through Eq. 5.

$$C = \left(\frac{\Delta V_o}{V_o} \right)^{-1} \frac{D_{nom}}{Rf} = 200 \mu F \quad \text{Eq. 5}$$

Table 5. Specific parameters for the charging converter.

Parameter	Description	Value
C	Capacitor	200 μF
D _{nom}	Nominal Duty Cycle	0.1461
Lm	Mutual Inductance	200 μH
N or (N1/N2)	Turn ratio	3
R	Converter Resistance	5 Ω

A similar approach is followed to design the discharging converter. In this case, a turn ratio (N) of 0.0333 was selected. The nominal duty cycle D_{nom} was calculated through Eq. 6, with the source voltage (V_s) corresponding to a single cell and the output voltage (V_o) corresponding to the module voltage. The required minimum mutual inductance (L_{mMin}) is calculated through Eq. 7. The mutual inductance (Lm) value chosen for the discharging converter was kept at the minimum value obtained in Eq. 7.

$$V_o = V_s \left(\frac{D_{nom}}{1 - D_{nom}} \right) \left(\frac{N_2}{N_1} \right) \quad D_{nom} = 0.4 \quad \text{Eq. 6}$$

$$Lm_{Min} = \frac{(1 - D_{nom})^2 R}{2f} \left(\frac{N_1}{N_2} \right)^2 = 4 \mu H \quad \text{Eq. 7}$$

The capacitance is calculated through Eq. 8. In this case, a voltage ripple of up to 1% was chosen, which yields a capacitor value (C) of 250 nF.

$$C = \left(\frac{\Delta V_o}{V_o} \right)^{-1} \frac{D_{nom}}{Rf} = 250 \text{ nF} \quad \text{Eq. 8}$$

Table 6. Specific parameters for the discharging converter.

Parameter	Description	Value
C	Capacitor	250 nF
D	Nominal Duty Cycle	0.4
Lm	Mutual Inductance	4 μ H
N (N1/N2)	Turn ratio	0.0333
R	Converter Resistance	400 Ω

3.2.3 Design of LC filter

An LC filter is added to the output of each DC-DC converter to smooth the immediate change in the cell current as a product of the cell series resistance. The basic structure of the filter is shown in Figure 20. The input of the filter is the output of one of the DC-DC converters, while the output is connected to the switch matrix, i.e., achieving a parallel connection to a battery cell.

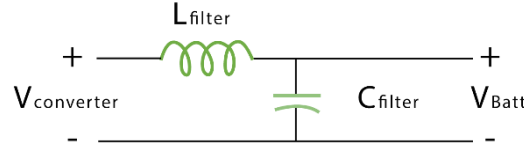


Figure 20. Structure of the LC filter.

A value of 60 dB has been chosen to generate an adequate attenuation A , while a value of 68 μ F is chosen for capacitor C_{filter} . By considering the switching frequency f_{sw} of the DC-DC converters, the equivalent impedance of the capacitor C_{filter} can be calculated through Eq. 9 [51]. Then, the desired equivalent impedance of inductor L_{filter} is obtained through Eq. 10. This value is then re-converted to inductance by using Eq. 11.

$$X_{C_{filter}} = \frac{1}{(2\pi)(f_{sw})(C_{filter})} = \frac{1}{(2\pi)(100 \times 10^3)(68 \times 10^{-6})} = 0.0234 \Omega \quad \text{Eq. 9}$$

$$X_{L_{filter}} = (X_{C_{filter}}) \left(10^{\frac{A}{20}} - 1 \right) = 23.3817 \Omega \quad \text{Eq. 10}$$

$$L_{filter} = \frac{X_{L_{filter}}}{(2\pi)(f_{sw})} = \frac{23.3817}{(2\pi)(100 \times 10^3)} = 37.213 \mu H \quad \text{Eq. 11}$$

The value of inductance of L_{filter} is then re-adjusted to 50 μH for simplicity. To calculate the resulting attenuation, Eq. 12 and Eq. 13 are then used. The final attenuation is 62.5651 dB, which is close to the initial requirement.

$$X_{L_{filter}} = (2\pi)(f_{sw})(L_{filter}) = (2\pi)(100 \times 10^3)(50 \times 10^{-6}) = 31.4159 \Omega \quad \text{Eq. 12}$$

$$A = 20 \log \left(\frac{X_{L_{filter}}}{X_{C_{filter}}} + 1 \right) = 20 \log \left(\frac{31.4159}{0.0234} + 1 \right) = 62.5651 \text{ dB} \quad \text{Eq. 13}$$

3.3 Proposed control loop

Since SoC is directly affected by the cell current, a higher balancing current could provide a faster means to achieve cell balance. However, higher currents can cause cells to fall out of the cell voltage and SoC limits. Therefore, to maximize balancing current without compromising cell integrity, it is proposed to incorporate the SoP (of the cell under balance) to adequately calculate the balancing current. The SoP of a cell can be expressed in its simplest form by Eq. 14, i.e., as the product of the cell terminal voltage (V) and the maximum allowable instant current ($I_{allowed}$) that can go through the cell without violating its operational limits.

$$SOP = VI_{allowed} \quad \text{Eq. 14}$$

SoP is traditionally calculated by first calculating the $I_{allowed}$, according to the operational limit of interest. Once the value of $I_{allowed}$ is obtained, SoP can be calculated by following Eq. 14. There are two approaches for calculating this current:

- Voltage-based: Calculates the maximum current that ensures that the cell voltage does not surpass the maximum cell voltage or falls below the minimum cell voltage.
- SoC-based: Calculates the maximum current that ensures that the cell will not surpass the maximum SoC or fall below the minimum SoC.

Besides these calculations, each cell has associated maximum discharging and charging current limits that need to be considered. Generally, both SoP calculations are run simultaneously, and the system chooses the current that is smaller in magnitude and falls inside the safe operational current limits. If the SoP-calculated current is larger than current limits, then the limits are used instead.

Calculations for the voltage-based SoP current are shown in Eq. 15 and Eq. 16, while calculations for the SoC-based SoP current are described in Eq. 17 and Eq. 18. It is worth noting that VOC and R_{Series} are SoC-dependent. Discharging current is considered positive, while charging current is considered negative. For SoC-based calculations, a period of charging (or discharging) of 1 second has been considered.

$$I_{DischargeMax} = \frac{VOC - V_{min}}{R_{Series}} \quad \text{Eq. 15}$$

$$I_{ChargeMax} = \frac{VOC - V_{max}}{R_{Series}} \quad \text{Eq. 16}$$

$$I_{DischargeMax} = \frac{SOC - SOC_{min}}{(t_{Discharge})(Capacity)(3600)} \quad \text{Eq. 17}$$

$$I_{ChargeMax} = \frac{SOC - SOC_{max}}{(t_{Charge})(Capacity)(3600)} \quad \text{Eq. 18}$$

To ensure that the adequate current is extracted or injected to the battery cells, each converter is controlled through two PI controllers, namely, PI current and PI voltage controllers. The PI current controller takes the balancing current reference, which in this case has been equaled to the passive balancing current, and calculates the error of the actual balancing current. This generates a new voltage reference that is fed to the PI voltage controller. This controller takes the current cell voltage and calculates the error, producing a new duty cycle reference for the converter. A block diagram of this control scheme is shown in Figure 21.

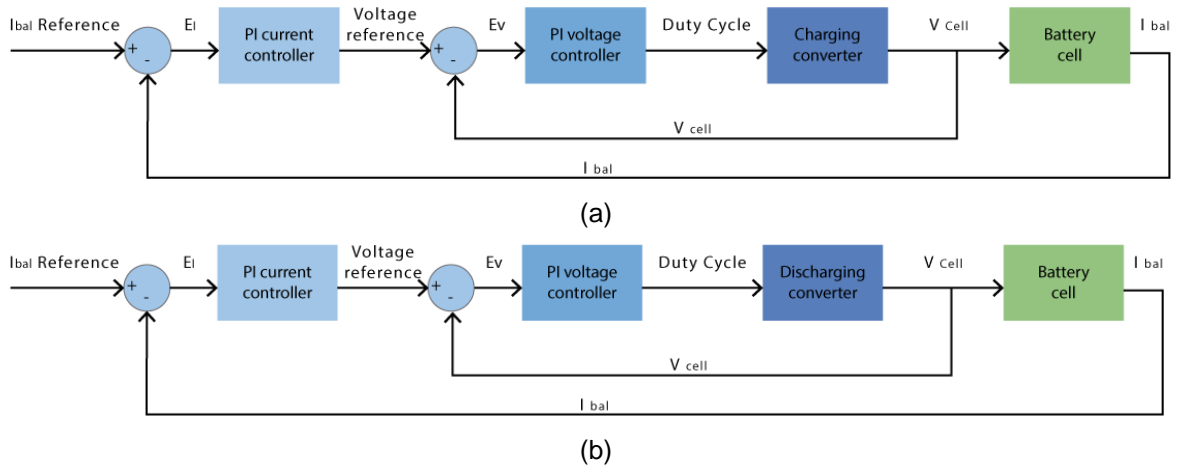


Figure 21. (a) Control loop for the charging converter, and (b) control loop for the discharging converter.

The general control loop is shown in Figure 22. Notice that the two DC-DC converters are shown connected to their respective PI controllers. Battery cell information is extracted through the different sensors, encapsulated as sensors block. This information is then processed by the balancing algorithm to determine which cell requires balancing, activating the adequate switches inside the switch matrix. The SoP current calculator calculates the balancing current reference, which is then fed to PI controller blocks to be used as a reference to regulate the converters to pursue cell balancing.

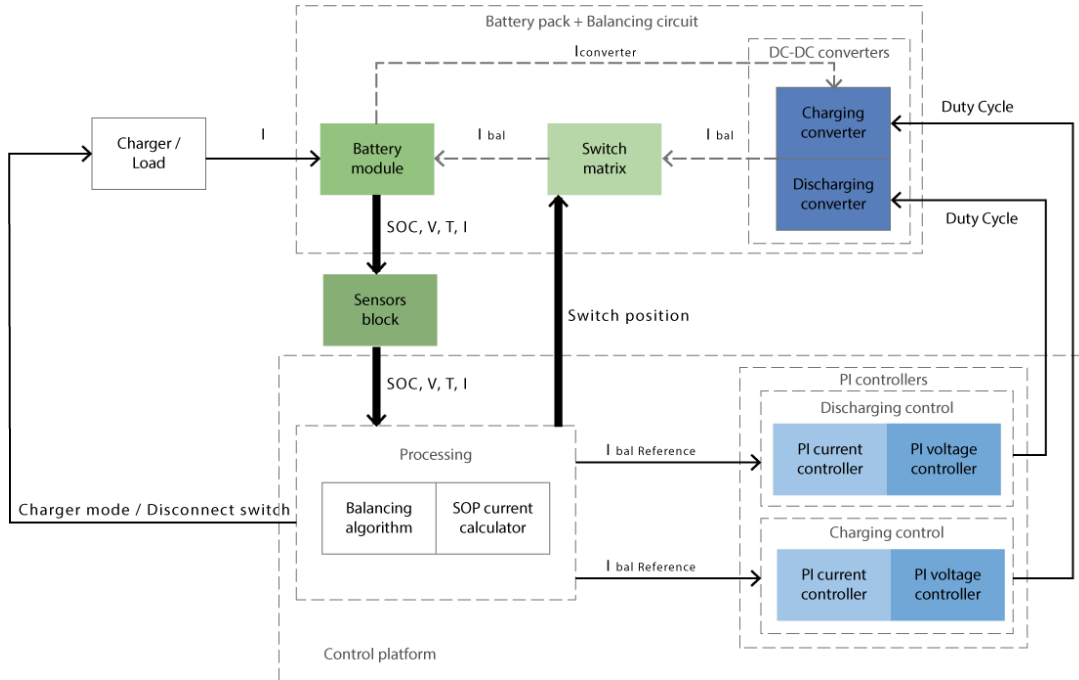


Figure 22. SoP-based control loop.

In Figure 22, dashed lines represent intermittent flow, as the converters can be turned off if the battery pack is balanced. This prevents current from flowing from the battery module to the converters and vice versa. Solid thin lines represent simple information flow, while thicker solid lines represent bus connections, which consists of more than one variable.

3.3.1 Design of PI controllers

To ensure that the DC-DC converters provide the adequate balancing current, four PI controllers were implemented and configured in the battery simulation framework, developed in the Simulink™ environment. As previously explained, each DC-DC

converter is controlled by a cascade connection of two PI controllers forming two loops, namely, an inner and outer loop. The outer loop controls current, while the inner loop is in charge of the voltage control. Eq. 19 shows the PI controller for the current loop,

$$\frac{V_{ref}}{E_I} = K_{P,I} + K_{I,I} \frac{1}{s} \quad \text{Eq. 19}$$

where V_{ref} stands for the voltage reference to be fed to the voltage loop controller, E_I represents the error between the measured current and the reference balance current generated by the SoP calculation, $K_{P,I}$ and $K_{I,I}$ are the proportional and integral gain constants for the current loop, respectively.

On the other hand, Eq. 20 presents the PI controller for the voltage loop,

$$\frac{D_{ref}}{E_V} = K_{P,V} + K_{I,V} \frac{1}{s} \quad \text{Eq. 20}$$

where D_{ref} is the duty cycle reference to be injected to the corresponding DC-DC converter, E_V corresponds to the error between the voltage reference generated by the current loop and the actual cell voltage, while $K_{P,V}$ and $K_{I,V}$ are the proportional and integral gain constants for the voltage loop, respectively.

3.3.2 Tuning of the PI controllers

The process of tuning the PI controllers has been performed under the following assumptions:

1. Tuning the PI current controllers: This controller has a direct relation to the dynamics of the battery cell. As the battery cell has a very slow voltage dynamic response, the voltage input to the cell can be considered as a constant filtered by the LC filter at the output of the DC-DC converters. Therefore, the output of the PI current controller, which is a voltage reference for the PI voltage controller, is translated by the battery cell into a current. To tune the PI current controller, only the dynamics of the battery cell and LC filter are considered.
2. Tuning the PI voltage controllers: The voltage controller has a direct impact on the dynamics of the DC-DC converter. The current reference generated by the PI current controller can be considered as a constant for the PI voltage controller.

As the battery cell has slow voltage dynamics, the PI voltage controller has a larger impact on the DC-DC converter. Therefore, only the DC-DC converters are considered for tuning the PI voltage controllers.

3.3.3.1 Tuning the PI voltage controller for the charging converter

A simple simulation of the charging converter described in section 3.2.2 operating in an open-loop was performed to get its step response. The simulation was conducted for 2 seconds, with a step from a Duty Cycle of 0.15 to 0.20 (Δu) at the 1 second mark, causing a change (Δy) of 2.148 V in the output of the converter. To estimate the controller constants, the guidelines presented by Skogestad were followed [52]. First, system parameter k was deduced from the change in output and input during the step response, as shown by Eq. 39. Then system constant τ_1 (shown in Eq. 22) was calculated as the point in time, where the output reaches 63% of its final value. After that, parameter k' was calculated as explained in Eq. 23. Then tuning parameter τ_c was selected as 0.015 to provide a robust and fast enough closed-loop response. Controller constants $K_{P,V}$ and $K_{I,V}$ were then calculated as shown in Eq. 24 and Eq. 25. To keep the charging converter response within adequate limits, the output was bound between 0.1 and 0.2. These boundaries limit the output of the charging converter between 2.41 V and 6.37 V, according to Eq. 2.

$$k = \frac{\Delta y}{\Delta u} = \frac{2.148}{0.05} = 42.96 \quad \text{Eq. 21}$$

$$\tau_1 = 0.009 \text{ s} \quad \text{Eq. 22}$$

$$k' = \frac{k}{\tau_1} = \frac{42.96}{0.009} = 4773.33 \quad \text{Eq. 23}$$

$$K_{P,V} = \left(\frac{1}{k'}\right)\left(\frac{1}{\tau_c}\right) = \left(\frac{1}{4773.33}\right)\left(\frac{1}{0.005}\right) = 0.0013966 \quad \text{Eq. 24}$$

$$K_{I,V} = \frac{K_{P,V}}{\min(\tau_1, 4\tau_c)} = \frac{0.0013966}{\min(0.009, 0.06)} = 0.15518 \quad \text{Eq. 25}$$

Figure 23 shows a comparison between the open-loop response and the closed-loop response of the charging. The desired output value was fixed at 4.2 V. Note how the open-loop system delivers an unstable output at first that continues to oscillate during

steady-state response. On the other hand, the system coupled with the tuned controller provides a much more stable voltage output.

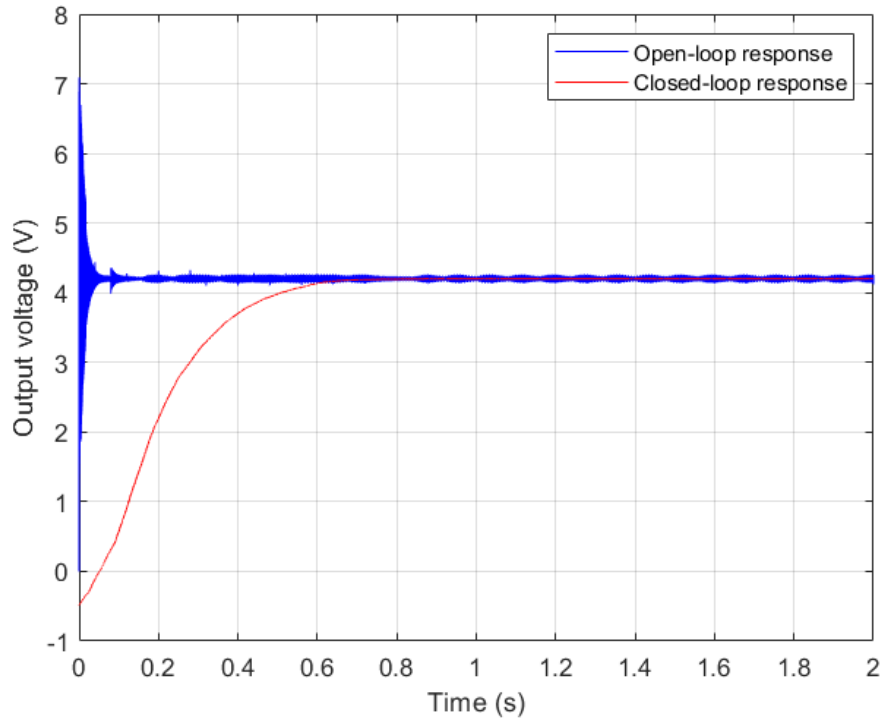


Figure 23. Comparison between open-loop and closed-loop response of charging converter for a desired output of 4.2 V.

3.3.3.2 Tuning the PI voltage controller for the discharging converter

Following a similar process as for the charging converter, an open-loop simulation of the discharging converter described in section 3.2.2 was run to evaluate its step response. The simulation was conducted for 2 seconds, with a step from a Duty Cycle of 0.15 to 0.20 (Δu) at the 1 second mark, causing a change (Δy) of 9.244 V in the output of the converter. First, system parameter k was deduced from the change in output and input during the step response, as shown by Eq. 26. Then system constant τ_1 (shown in Eq. 27) was calculated as the point in time, where the output reaches 63% of its final value. After that, parameter k' was calculated as explained in Eq. 28. Then tuning parameter τ_c was selected as 0.2 to provide a robust and fast enough closed-loop response. Controller constants $K_{P,V}$ and $K_{I,V}$ were then calculated as shown in Eq. 29 and Eq. 30. To keep the charging converter response within adequate limits, the output was bound between 0.1

and 0.45. These boundaries limit the output of the discharging converter between 13.34 V and 101.8 V, according to Eq. 6.

$$k = \frac{\Delta y}{\Delta u} = \frac{9.244}{0.05} = 184.88 \quad \text{Eq. 26}$$

$$\tau_1 = 0.0005 \text{ s} \quad \text{Eq. 27}$$

$$k' = \frac{k}{\tau_1} = \frac{184.88}{0.0005} = 369760 \quad \text{Eq. 28}$$

$$K_{P,V} = \left(\frac{1}{k'}\right)\left(\frac{1}{\tau_c}\right) = \left(\frac{1}{369760}\right)\left(\frac{1}{0.2}\right) = 0.0000135 \quad \text{Eq. 29}$$

$$K_{I,V} = \frac{K_{P,V}}{\min(\tau_1, 4\tau_c)} = \frac{0.0000135}{\min(0.0005, 0.8)} = 0.027 \quad \text{Eq. 30}$$

Figure 24 shows a comparison between the open-loop response and the closed-loop response of the discharging converter. The desired output value was fixed at 84 V. Note how the open-loop system delivers an output with some high overshoots, while the tuned closed-loop system provides a much more stable voltage output.

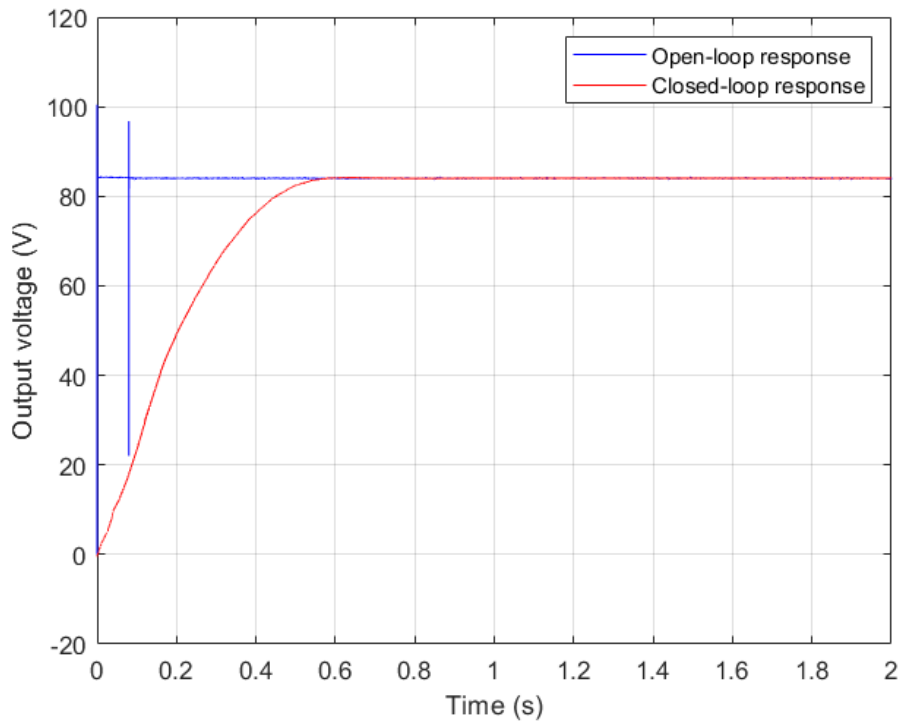


Figure 24. Comparison between open-loop and closed-loop response of the discharging converter for a desired output of 84 V.

3.3.3.3 Tuning the PI current controllers

As the system for both PI current controllers is the same, i.e., the same battery cells, the tuning of this controller must only be done once. Following a similar process as the one described for the tuning of the PI voltage controllers, an open-loop simulation of the battery cells was performed. To avoid complications that could tarnish the tuning process, the battery cell model was modified by removing the SoC dependence of the R_{Series} , $R1$, $C1$, and V_{OC} circuit components. Instead, the corresponding values for a 60% SoC were used.

As the battery cell receives the voltage output of the PI current controller as a constant with no dynamics (DC-DC converters were not considered for the tuning process), and due to the effect of the series resistor R_{Series} and the relatively large value of $C1$, the battery cell displays an immediate current response after a step in the voltage input. This response is largely dominated by the value of the difference between the voltage input and V_{OC} , divided by R_{Series} , as shown in Eq. 31. This current value decreases over a long period of time as Capacitor $C1$ gets saturated, converging to the value described in Eq. 32.

$$I_{Bal} = \frac{V_{ref} - V_{OC}}{R_{Series}} \quad \text{Eq. 31}$$

$$I_{Bal} = \frac{V_{ref} - V_{OC}}{R_{Series} + R1} \quad \text{Eq. 32}$$

To smooth the immediate response of the current against a change in the input voltage, an LC filter between the battery cell and the DC-DC converter output has been implemented as described in section 3.2.3. The addition of this filter allows the correct tuning of the PI controller.

An open-loop simulation of the battery cells was conducted by replacing the voltage loop by a controller voltage-source. The output of the voltage source is then connected to the LC filter, which is finally connected to one of the battery cells. The simulation was conducted for 2 seconds, with a step of voltage input from 4.2 to 4.25 (Δu) at the 1 second mark, causing a change (Δy) of 0.775529 A in the current of the cell. System parameter k was deduced from the change in output and input during the step

response, as shown by Eq. 33. Then system constant τ_1 (shown in Eq. 34) was calculated as the point in time, where the output reaches 63% of its final value. After that, parameter k' was calculated as explained in Eq. 35. Then tuning parameter τ_c was selected as 0.15 to provide a robust closed-loop response. This parameter has been fixed at a larger value than the parameters chosen for the voltage-loop. Controller constants $K_{P,V}$ and $K_{I,V}$ were then calculated as shown in Eq. 41 and Eq. 37. To keep the battery cell response within adequate limits, the output of the PI current controllers was bound between 3.6 V and 4.25 V. These limits ensure adequate protection for the operation of the battery cells.

$$k = \frac{\Delta y}{\Delta u} = \frac{0.775529}{0.05} = 15.5106 \quad \text{Eq. 33}$$

$$\tau_1 = 0.00076 \text{ s} \quad \text{Eq. 34}$$

$$k' = \frac{k}{\tau_1} = \frac{15.5106}{0.00076} = 20408.6579 \quad \text{Eq. 35}$$

$$K_{P,V} = \left(\frac{1}{k'}\right) \left(\frac{1}{\tau_c}\right) = \left(\frac{1}{20408.6579}\right) \left(\frac{1}{0.15}\right) = 0.0003267 \quad \text{Eq. 36}$$

$$K_{I,V} = \frac{K_{P,V}}{\min(\tau_1, 4\tau_c)} = \frac{0.0003267}{\min(0.00076, 0.6)} = 0.429814 \quad \text{Eq. 37}$$

Figure 25 shows a comparison between the open-loop response and the closed-loop response of the balancing current. The desired balancing current value was fixed at 0.5 A. Note how although the open-loop system delivers a stable output at the beginning, the balancing current value decreases over time as the VOC of the battery cell starts increasing due to the cell being charged, as shown by Eq. 31. On the other hand, the closed-loop system is capable of providing a stable balancing current during the whole simulation, as it updates the reference voltage value appropriately.

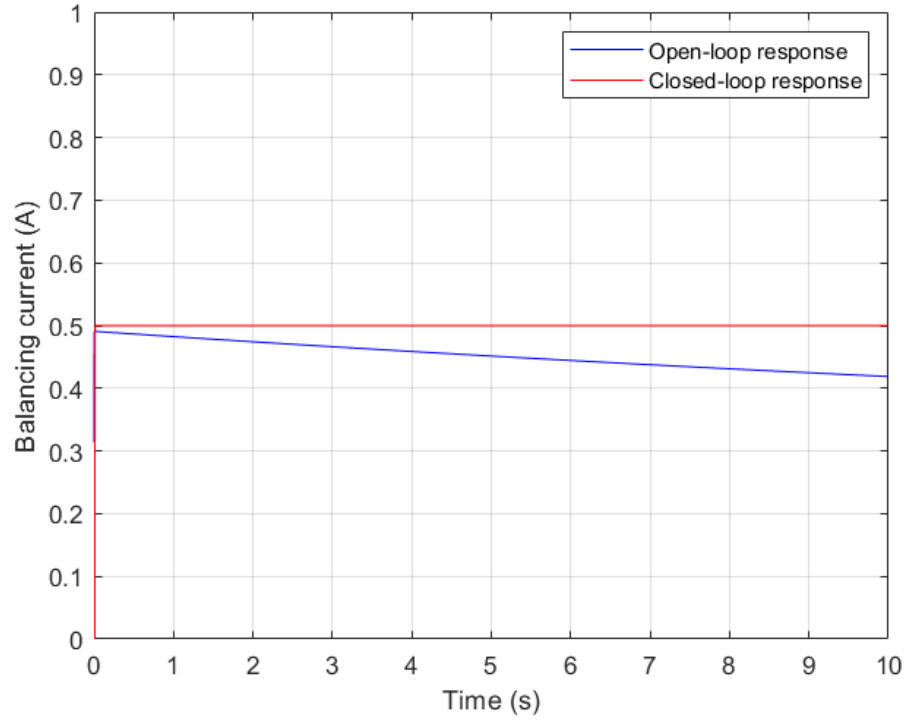


Figure 25. Comparison between open-loop and closed-loop response of the resulting balancing current for a value of 0.5 A.

3.3.3.4 Parameters for the PI voltage and current controllers

Table 7 shows the tuned parameters of each PI controller, after following the processes described in previous sections.

Table 7. Parameters for the PI controllers used in the simulations.

DC-DC converter	Control loop	K_P	K_I
Charging	Voltage	0.0013966	0.1552
	Current	0.0003267	0.4298
Discharging	Voltage	0.0000135	0.027
	Current	0.0003267	0.4298

3.4 Development of the balancing algorithm

This segment explains the process behind the development of the proposed MFCSA. One of the limitations of this active balancing topology is that only one cell can be balanced at a time. This means that each converter can only be connected to one cell

at once, which contrasts with passive balancing systems, where multiple cells can be balanced at a time.

3.4.1 Multi-factor cell selection algorithm (MFCSA)

Balancing algorithms generally consider only one variable, either voltage or SoC. However, this can lead to bad performance under varying cell parameters and can also generate a slow response. Therefore, a new algorithm to select the cells to be balanced is proposed here.

The proposed algorithm is based on the work of Piao et al. [21], which is built on the distance outlier detection. This methodology is able to consider more than one parameter to determine which cells need a balancing action, either increasing its charging current or delivering its charge to other cells (or resistors). The algorithm follows the next steps:

1. Calculate standardized z-score for each cell parameter.

$$Z_{ij} = \frac{Cell_{ij} - \overline{Cell}_j}{\delta_j} \quad \text{Eq. 38}$$

$$\overline{Cell}_j = \frac{\sum_{i=1}^n Cell_{ij}}{n} \quad \text{Eq. 39}$$

$$\delta_j = \sqrt{\frac{\sum_{i=1}^n (Cell_{ij} - \overline{Cell}_j)^2}{n - 1}} \quad \text{Eq. 40}$$

2. Determine distance of the cells to all other cells, based on z-scores.

$$D(Z_m, Z_n) = \sqrt{|Z_{m1} - Z_{n1}|^2 + |Z_{m2} - Z_{n2}|^2} \quad \text{Eq. 41}$$

3. Calculate the outlier value of each cell by summing the distances of each cell.

$$W(Z_m) = \sum_{m=1}^n \sum_{j=1}^2 D(Z_m, Z_n) \quad \text{Eq. 42}$$

4. Calculate the outlier threshold and check if the outlier value of a cell surpasses it.

$$VOA1 = \frac{\sum_{m=1}^n W(Z_m)}{n} \quad \text{Eq. 43}$$

5. Select the cell with the lowest outlier value as the centroid for normal performing cells and the cell with the highest outlier value as the centroid for the abnormal performing cells.

6. Calculate the distance of each cell to the centroids and classify them as either normal or abnormal.
7. Calculate the error of each cell to the centroid and sum the errors.

$$J_m = \sum_{m=1}^{N_m} \|Z_m - C_j\|^2 \quad \text{Eq. 44}$$

$$J_e = \sum_{j=1}^k J_m = \sum_{j=1}^k \sum_{m=1}^{N_m} \|Z_m - C_j\|^2 \quad \text{Eq. 45}$$

8. Re-calculate the centroids considering all cells in the classification.
9. Iterate steps 6-8 until a global minimum for the cumulative error is reached.
10. Cells classified as abnormal are to be selected for the balancing operation. The specific operation will depend on the status of the cells.

The algorithm can be further explained using the flow diagram shown in Figure 26:

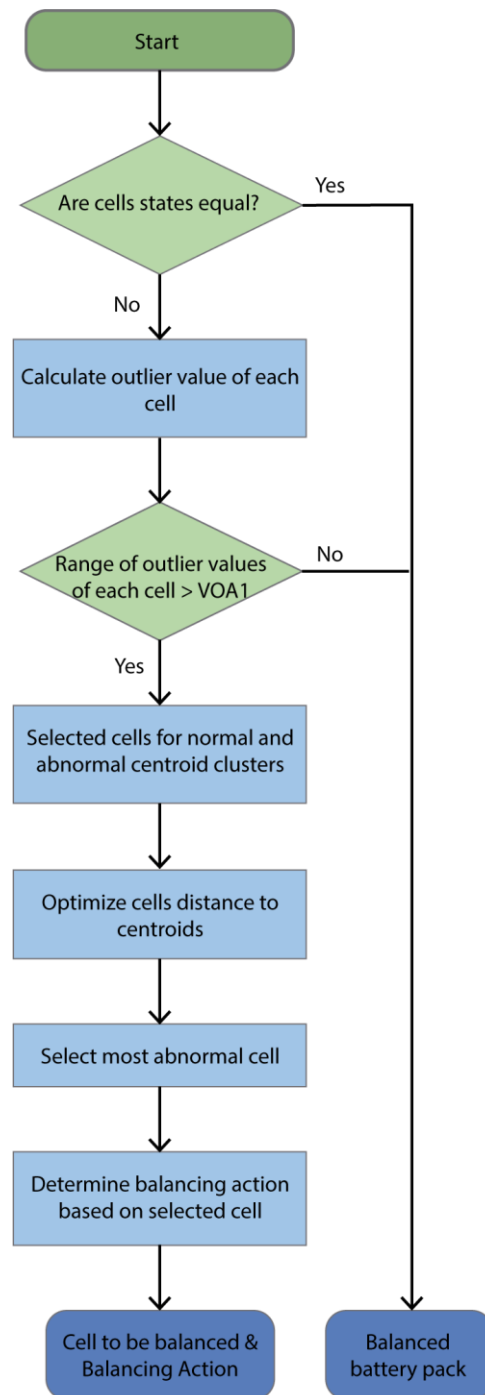


Figure 26. Algorithm for selection of cells that require a balancing operation.

Extending on the idea proposed by Piao et al. a new MFCSA was developed [21]. The distance-based algorithm was implemented in Simulink™, using SimScape™ and Stateflow™ blocksets and using the battery electrical models already established, as well as the CCCV charging scheme. The algorithm was configured to consider up to three

different balancing factors. Once the cell information is fed to the MFCSA, the output provides the appropriate values to control the switches that connect a determined battery cell to the balancing module.

To ensure safe operation of the battery pack, appropriate means to check whether temperature or voltage have exceeded safe operational limits were added to balancing algorithm. When these limits are trespassed, the charger stops operating by controlling a logic switch added to disconnect the energy source from the battery pack. It is important to note that the upper cell voltage limit has been set to 4.25 V. Besides, charging also is programmed to stop once one of the cells reaches 100% SoC or when the least charged cell reaches 100% SoC within certain tolerance controlled by a variable called *deltaSoC* to prevent overcharging.

The whole balancing algorithm along with the safety checks can be seen in Figure 27. Here, it is shown how the algorithm can enter to the *disconnect* mode at any time if a cell voltage or SoC exceed the safety limits. The system can resume to charging mode once a minute has passed and the readings are below the maximum safety limit.

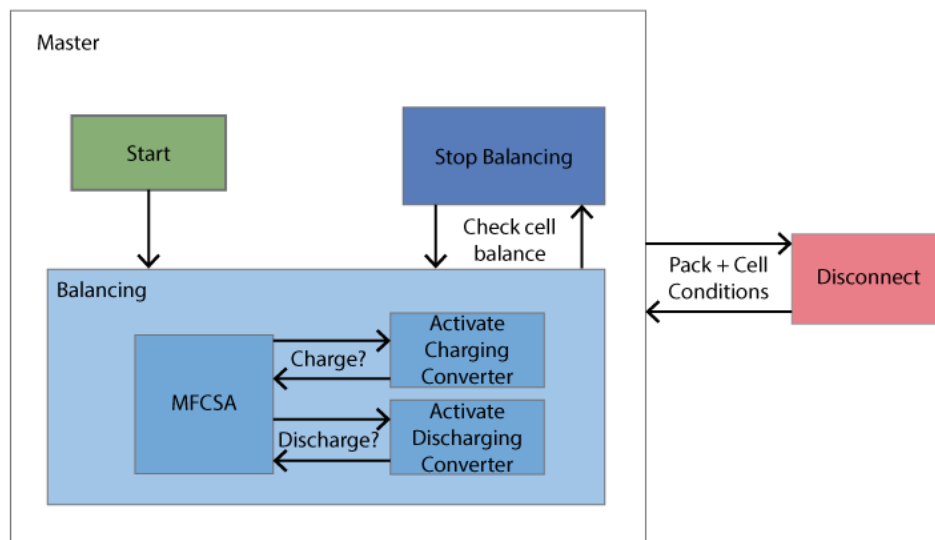


Figure 27. Proposed balancing algorithm with safety checks.

The new balancing algorithm comprises the following stages:

- A. Master: Contains the cell selection algorithm and operates while cell and pack conditions are within safe limits. It is divided into more sub-stages:
 1. Start: All balancing modules are disconnected, i.e., all switches are set to 0.

2. Balancing: MFCSA function is started to determine which cells need balancing (either injecting extra charge or to liberate excess of charge). Depending on the results of MFCSA, the adequate DC-DC Converter is selected. Values are updated every 5 seconds.
 3. Stop balancing: If no switch needs to be activated based on the results of the MFCSA function, each switch is set to 0. MFCSA function is run every 5 seconds in this stage. If the result prompts the system to turn on one of the switches and one of the cells SoC is different from the others by a value larger than the tolerance, then the algorithm enters to the *balancing* mode once again.
- B. Disconnect: This status can be achieved after the charging process has been finalized or an unsafe condition was achieved. If during operation it is detected that a cell has a voltage over 4.25 V, then the system deactivates the balancing modules and the master switch, disconnecting the energy source from the battery pack. System conditions are evaluated once every minute to determine if the operation can resume. If one of the cells reaches 100% SoC, then the master switch is also disconnected. Charging also stops if the least charged cell reaches full charge within tolerance. In this stage, balancing modules are also disconnected.

3.4.2 Balancing factors

To improve the performance of the basic single factor balancing algorithm, a multi-factor balancing scheme was developed as explained in previous sections. Three different balancing factors were considered:

1. SoC: The actual state of charge of each cell, assuming that this quantity is exactly known at any given time.
2. Voltage: The terminal voltage varies quickly depending on the current flowing through the cell and due to the effect of the internal resistance R_0 . Therefore, using this measurement for balancing can result in instability. Thus, VOC was chosen instead, as it changes slowly during the whole cycle.

3. SoE: Absolute remaining energy was also chosen as a balancing factor. As for the SoC, the algorithm assumes that the actual SoE is known at any given time.

Every balancing factor is assigned a weight, which determines its influence on the output of the balancing algorithm. The sum of the individual weights must be equal to 1. Chapter 4 includes the results from simulations using different iterations of the proposed balancing weights.

Chapter 4

Numerical evaluation of proposed system

This chapter explains the simulation conditions and numerical results obtained of the proposed balancing system in the developed battery simulation framework.

4.1 Simulation environment

A Li-ion cell was characterized using the data from the RW discharge experiments presented by Bole et al. [45]. The characterization was performed in Matlab™ according to the procedure described in Appendix I. A module of 20 cells was implemented using SimScape™ blocks inside the Simulink™ environment. The proposed active balancing circuit was also implemented in Simulink™ using SimScape™ blocks, while, for comparison purposes, a passive balancing circuit for reference was developed using the same simulation environment. Stateflow™ was used to control the execution of the simulation, and to implement the proposed MFCSA, as well as other basic balancing algorithms. The proposed control loop was executed using Simulink™ blocks.

4.2 Simulation conditions

This section presents the conditions under which the proposed balancing system was simulated are exposed.

4.2.1 Charging profiles

Two different charging profiles have been implemented to test the function of the proposed balancing system. The first one corresponds to the *constant current constant voltage* (CCCV) approach, while the second one corresponds to *pulsed constant voltage* (PCV) charging scheme. To prevent the unbalanced cells to reach maximum voltage before the others, a maximum constant voltage of 83 V has been fixed, instead of the maximum module voltage of 84 V. This condition avoids overcharging cells with a significantly smaller capacity than others.

4.2.1.1 CCCV charging profile

The CCCV scheme consists of a constant current control stage followed by a constant voltage control stage. The system switches between the two stages once a

threshold voltage has been reached. The voltage source of the CV section was set to 4.15 V/cell to comply with the requirements of these cells. Besides, the CC portion was set to use a rate of 0.33C. The transition between the CC and CV stages is controlled by the battery pack voltage. When the voltage of the pack reaches 83 V, the controlled current source is disconnected, while the constant voltage source begins operation, keeping a constant voltage of 83 V through the rest of the charging operation. Once the charging current reaches a magnitude of 1/10 C rate, the charger is disconnected from the battery pack. It is then assumed that the battery pack has been fully charged.

4.2.1.2 PCV charging profile

This method consists on feeding the battery pack with voltage pulses of constant amplitude equal to the top charging voltage (4.15 V/cell for these cells), with a duty cycle adjusted to achieve a balance between charging time and temperature rise. For simplicity, a fixed duty cycle of 50% has been used for simulation [44]. Similar to the CCCV charging scheme, a top voltage of 83 V has been fixed for this charging scheme. Pulses of 83 V with a period of 60 seconds and 50% duty cycle are injected to the battery pack. Once the resulting charging currents are below 1/10 C rate, the charging system is disconnected. The battery pack is assumed to be fully charged.

4.2.2 Discharging profiles

Two different operational profiles have been implemented in the system simulation. The first one corresponds to an agricultural tractor driving profile, which was obtained from the EPA website [53]. This profile has a log of the percentage of speed and torque during a cycle comprising 629 seconds. A power profile was derived from both logs and scaled to the nominal power of the cell module (Eq. 46, Eq. 47). Out of this, a current demand profile based on the actual module voltage was obtained as shown in Eq. 48.

$$Power (\%) = (Speed \%)(Torque \%), \quad \text{Eq. 46}$$

$$P_{nom} = (V_{nom})(C_{nom}) = 131.9832 \text{ Wh}, \quad \text{Eq. 47}$$

$$I = \frac{(P_{nom})(Power (\%))}{V_{module}}. \quad \text{Eq. 48}$$

The corresponding speed and torque curves are shown in Figure 28, while the power and current profiles can be seen in Figure 29. For this representation, a constant voltage was used for power and current calculations; however, in the simulations, the actual module voltage was used.

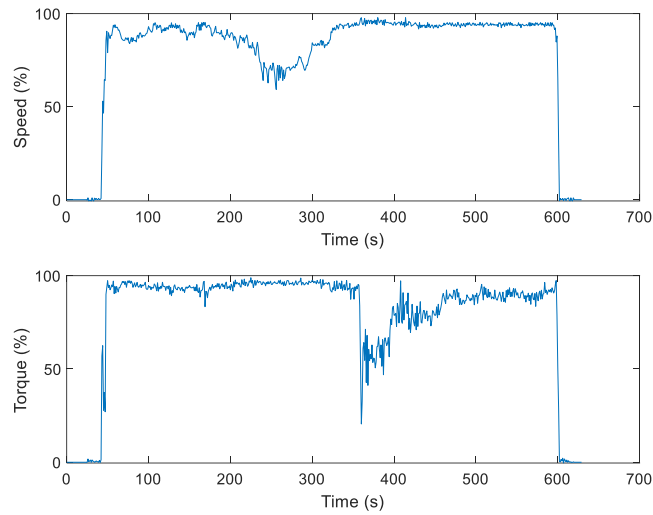


Figure 28. Speed and torque of the EPA agricultural tractor driving cycle [53].

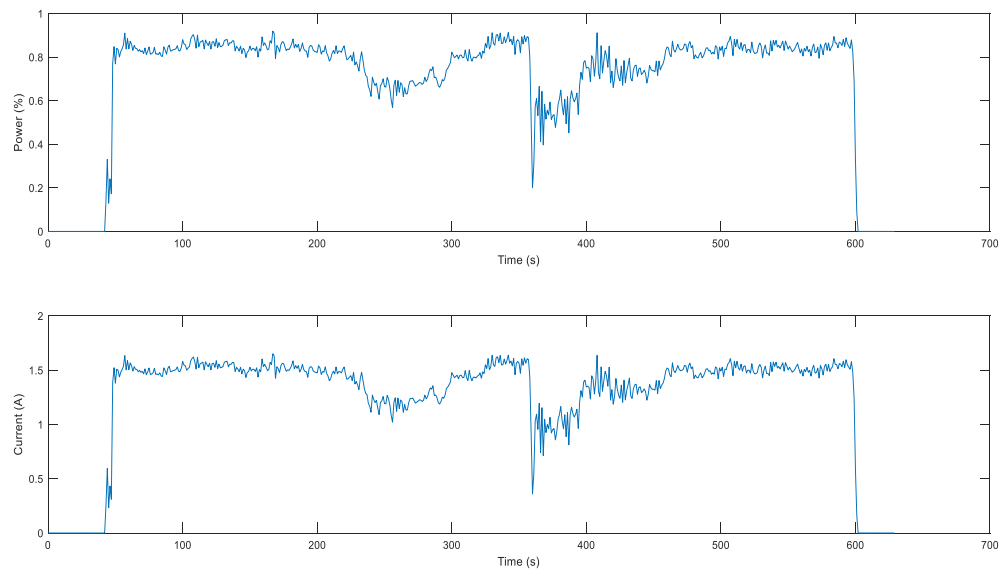


Figure 29. Power and current curves derived from the EPA agricultural tractor driving cycle.

Additionally, a speed and torque profile from a residential mower with a duration of 1 hour was also considered. The power and current curves were derived following a similar process as above. Figure 30 shows the power profile obtained from this process.

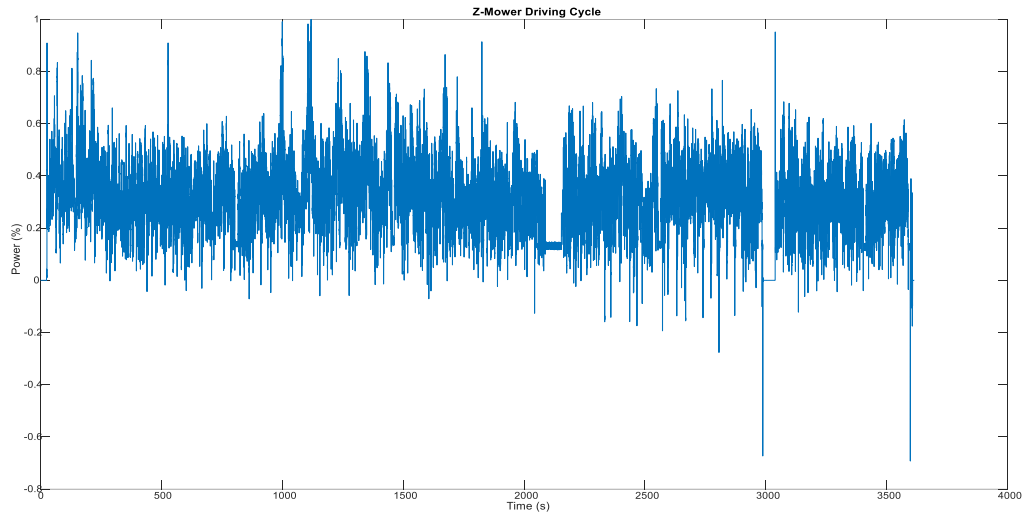


Figure 30. Power profile obtained from the residential mower driving cycle.

It is worth to note that the power profile of the EPA agricultural tractor seems to lean towards higher power percentages, while the residential mower profile leans towards lower percentages. From this, a longer runtime can be expected from the residential mower profile, as the battery module will constantly experiment lower currents.

4.2.3 Simulation cycle

A cycle consisting of three different periods is considered for the simulation of the balancing system:

- Initial charging: Cells are initialized to around 60% SoC and randomly varied between $\pm 5\%$ to induce a factory imbalance. Cells are then charged for up to 8000 seconds with a CCCV or PCV charging profile.
- Online operation: The cells are then discharged by using several instances of the discharging profiles. For the EPA cycle, 15000 seconds are allocated for this operation, while for the residential mower cycle, a time of 21000 seconds is considered.

- Second charging: The cells are then charged to full charge once again. This stage has a fixed duration of 13000 seconds.

4.2.4 Balancing schemes

For benchmarking purposes, cells were simulated using three different balancing approaches:

- No balancing.
- Passive balancing (enabled only during charging).
- The proposed active balancing system.

4.2.5 Cell conditions

To represent varying cell parameters due to manufacturing tolerances and inaccuracies, all cells parameters R_0 , R_1 , C_1 , and Capacity are varied within $\pm 5\%$ of their nominal value. Accordingly, their initial SoC was varied within $\pm 5\%$ of the initial SoC setpoint, which has been set at 60%. To represent cells at different points of their life-cycle, the capacity of 10 cells was decreased 20% of their initial nominal value.

4.3 Simulation results

Each of the following sections presents a specific aspect of the simulation results for comparison.

4.3.1 Analysis on charging and discharging times

The *charging time* has been defined as the time it takes the charging system to inject a current below $1/10$ C rate to the battery pack. However, in special situations where some of the cells have been aged considerably and no balancing system has been implemented, the charging may stop before reaching the aforementioned current rate, as some of the cells may reach their top voltage. In contrast, the *runtime* is the time it takes for one of the cells in the battery pack to reach its minimum allowed SoC. For these tests, the minimum allowed SoC has been set at 10%.

Since the simulation cycle is composed of two charging periods and one discharging period, two measurements for charging time and one for discharging time have been considered. The results from the simulations are condensed in Table 8. In this table, “charging time 1” and “charging time 2” represent the first and second charging periods, respectively, while “runtime” stands for the discharging period. The results from each balancing scheme have been compared to the simulations results obtained in the system without a balancing method.

Table 8. Charging time and runtime results from simulations under passive and the proposed active balancing schemes compared to simulations without a balancing system.

Balancing scheme	Charging time 1 (%)	Charging time 2 (%)	Runtime (%)
Passive	26.93	30.80	-3.57
Active	20.92	21.99	13.89

As shown in Table 8, the charging times have increased for both the passive and active balancing systems. This is due to the fact that the battery pack is now able to accept more energy, as aged cells reach their top voltage at a later time, which is a consequence of achieving a better balance when compared to the rest of the cells. Nonetheless, the increase in the charging times of the active balancing scheme is smaller than the one observed in the passive balancing scheme, as the energy injected into the battery pack is better distributed into the cells in the active scheme, instead of being dissipated in some other elements. As a consequence, the runtime is considerably increased with the active balancing scheme when compared to the unbalanced battery pack.

4.3.2 Analysis on energy efficiency

The energy injected into the battery pack was obtained after subtracting the energy dissipated in the balancing system (resistors, DC-DC converters, switches) from the energy distributed by the charging system. Additionally, the energy that could be extracted from the battery pack has also been measured. Table 9 shows an average of the results from the different simulations including the CCCV and PCV charging schemes, as well as the results obtained considering the EPA and residential mower discharging

profiles. In this table, “energy in 1” and “energy in 2” stand for the two charge periods, respectively, while “energy out” represents the energy extracted from the battery pack during the discharge period.

Table 9. Energy results from simulations under different balancing schemes.

Balancing scheme	Energy in 1 (Wh)	Energy in 2 (Wh)	Energy out (Wh)
No balancing	47.20	105.45	96.56
Passive	49.61	101.92	93.03
Active	49.65	117.98	109.61

The injected and extracted energy results of the simulations under the passive and the proposed active balancing scheme have been compared to the data obtained from the simulations of the battery pack without balancing. This comparison has been laid out in Table 10. The basis for the calculations of the percentages are the energy results shown in Table 9, with the results from the simulations without balancing taken as the reference. Furthermore, “energetic efficiency” represents the proportion of energy injected by the charger that was effectively distributed into the battery cells, i.e., not dissipated in other elements.

Table 10. Energy results from simulations under passive and the proposed active balancing schemes compared to simulations without a balancing system.

Balancing scheme	Energy in 1 (%)	Energy in 2 (%)	Energy out (%)	Energetic efficiency (%)
Passive	5.27	-3.35	-3.66	85.24
Active	5.36	11.88	13.53	99.81

Notice that the proposed active balancing system ensures that more energy is injected into the cells, which correlates with the longer runtime during discharge. Accordingly, the energy extracted from the battery pack is also considerably larger with the proposed active balancing method. Notice that, although the passive balancing method managed to inject more energy during the first charge period, this extra energy could not be efficiently used by the cells during discharge. As a consequence, some cells

reach their SoC lower limit prematurely during discharge, which in its turn prevents some cells to be fully charged during the second charge period.

The proposed active balancing method showed a high energetic efficiency with only a small proportion of loss, which are mainly due to the switching and conduction losses in the DC-DC converters and switches required to connect them to the battery cells. In contrast, the passive balancing method showed a poor energetic efficiency as a high amount of energy was dissipated in the balancing resistors. It is important to note that the active system operated during both charge and discharge processes, while the passive system was only operative during the charge process.

4.3.3 Analysis on cell balancing

The SoC of each cell in the battery pack was calculated by integrating the current going through each cell and updating the initial SoC value, which was assigned at the start of the simulation. After each simulation, the SoC values of each cell were inspected to detect the cells with the lowest and highest SoC, and to calculate the mean SoC. The information gathered from the simulations has been averaged and condensed in Table 11. The “min” column shows the average of the cells with the lowest SoC at the conclusion of each period, while the “max” column shows the mean of the cells with the largest SoC. Additionally, the “mean” column displays the average SoC value obtained by aggregating the mean SoC value from each individual simulation.

Table 11. Balancing results from simulations under different balancing schemes.

Balancing scheme	Charging period 1			Charging period 2			Discharging period		
	Min (%)	Mean (%)	Max (%)	Min (%)	Mean (%)	Max (%)	Min (%)	Mean (%)	Max (%)
No balancing	87.65	92.83	99.70	87.65	92.83	99.70	10	17.34	23.08
Passive	92.93	93.89	95.14	93.09	93.89	94.88	10	21.83	28.56
Active	93.17	93.90	94.85	93.32	93.92	94.54	10	10.94	11.66

As expected, the system with no balancing displayed the highest degree of imbalance between the SoC values of the battery cells during the charging process,

characterized by a large difference between the maximum and minimum values, evidenced by a difference of 12.05% SoC after each charging period. In comparison, the proposed active balancing scheme displays a difference of 1.68% SoC after the first charging period, 1.22% SoC after the second charging period, while the passive balancing scheme shows a difference of 2.21% SoC for the first charging period, and 1.79% SoC for the second charging period. Notice that the mean SoC value during charging is not so different across the three balancing schemes. In contrast, there are some noticeable differences in the discharging section, where the proposed active balancing scheme displays a difference of 1.66% SoC between the fullest and emptiest cells, while the passive balancing scheme and unbalanced battery pack show a difference of 18.56% and 13.08% SoC, respectively.

Even though the passive and active balancing systems reached a similar mean SoC (93.89% and 93.90%, respectively) and balance during charging, since for both cases the difference between the highest and lowest SoC is below 2.5%, the proposed active scheme was able to ensure a tighter balance during discharge. This is revealed by the difference of 1.66% SoC for the proposed active balancing scheme and 18.56% SoC for the passive balancing scheme. This characteristic enables a longer runtime as the energy in each cell is distributed better among aged cells, preventing them from reaching the minimum allowed limit of SoC.

Chapter 5

Conclusions and future work

Li-ion cells have become a key component of several products, ranging from consumer electronics to industrial and commercial vehicles. However, to exploit their benefits in an optimal way, equipment manufacturers need to implement the appropriate means for balancing and equalizing the cells in the battery pack of their product. Not doing so may lead to a detrimental performance and may impact the battery service life seriously. Nowadays, most providers have implemented traditional passive balancing systems, which exhibit good balancing, but impact the energetic efficiency of the system by dissipating energy. Furthermore, they cannot operate during discharge, as more energy would be consumed, which severely limits the range of the vehicle or any other system fed by batteries. Active balancing systems, which redistribute energy instead of dissipating it, have also been explored in the literature, but their high implementation costs and complexity have limited their usage.

This work proposed an active balancing system that targets lower implementation costs, high robustness and fast balancing. The proposed system was composed by two DC-DC converters and one switch per battery cell. One of the converters extracted excess of energy from an overcharged cell and redirected it into the battery package; while the other converter took extra energy from the battery pack and injected into a discharged cell. This circuit contrasts with other active schemes, where one bidirectional converter per battery cell is included, thus reducing the amount of parts and system complexity.

A cell selection algorithm for balancing was also presented in this work, referred to as the multi-factor cell selection algorithm (MFCSA). It was shown that, the MFCSA increased the robustness of the system by enabling a multitude of states or variables to be considered when selecting a battery cell for a balancing operation. This algorithm weights state of charge (SoC), terminal voltage, and state of energy (SoE) to define which battery cell needs to be connected to the balancing circuit. The usage of multiple inputs has prevented the system from an excessive switching, which contributes on reducing the stress on aged cells.

Modern balancing systems are set to balance cells at fixed C rates, depending on the application and the nature of the battery cells. However, an improved control loop based on state of power (SoP) has been introduced as part of the proposed balancing system to accelerate the balancing speed. With the use of the SoP, the system can inject the maximum allowable current to a cell without damaging it and keeping its voltage and SoC inside safe operational limits. As opposed to use of fixed C rates, the proposed control loop maximizes the current that a charged cell can deliver and the current that a discharged cell can receive. This is reflected by the possibility of the system to expand the runtime of the application, which is due to the fact that the energy in the battery pack is distributed better among cells during online operation. Besides, the energy that can be injected into the battery pack during charging has also been increased, which is the consequence of moving the excess of energy from the overcharged cells to the rest, before anyone of them reaches its top voltage.

As part of future work, the proposed active balancing system could be implemented physically and tested in different scenarios and with battery packs of diverse characteristics and chemistries. Further tests could also include tests on commercial products. Subsequent research will need to consider how this balancing system can be introduced into an existing or a new BMS, ensuring compatibility between the control and balancing routines.

This work provides the foundation for further research in the area of active balancing systems. Several improvements have been identified and are listed as follows:

- The proposed algorithm only considered one cell for balancing operation. As the system has two converters, the algorithm could be further expanded to identify two cells for balancing, one to be connected to the charging converter and one to the discharging converter.
- Other battery cell parameters or states can also be introduced to the proposed algorithm MFCSA. For instance, state of health (SoH) can also be considered.
- The balancing strategy could be further optimized by planning the adequate switch and converter sequence by considering fixed charging profiles.

- Changes in the balancing circuit could be introduced, so that one converter can be connected to more than one cell at the time if needed, which may increase the balancing speed.

Chapter 6

Bibliography

- [1] G. Pistoia, "Lithium-Ion Batteries - Advances and Applications," in *Lithium-Ion Batteries - Advances and Applications*, 1st ed., Elsevier, 2014.
- [2] F. Altaf, B. Egardt and L. Johannesson Mårdh, "Load Management of Modular Battery Using Model Predictive Control: Thermal and State-of-Charge Balancing," *IEEE Transactions on Control Systems Technology*, vol. 25, no. 1, pp. 47-62, 2017.
- [3] F. Ran, H. Xu, J. Qin and W. Li, "An active balancing circuit for lithium battery management system with optoelectronic switches," in *TENCON 2015 - 2015 IEEE Region 10 Conference*, 2015.
- [4] D. Park, S. Choi, R. Kim and D. Kim, "A novel battery cell balancing circuit using an auxiliary circuit for fast equalization," in *IECON 2014 - 40th Annual Conference of the IEEE Industrial Electronics Society*, 2014.
- [5] V. Pham, T. Nguyen, D. Tran, V. Vu and C. Woojin, "A new cell-to-cell fast balancing circuit for Lithium-Ion batteries in Electric Vehicles and Energy Storage System," in *2016 IEEE 8th International Power Electronics and Motion Control Conference (IPEMC-ECCE Asia)*, 2016.
- [6] F. S. Hoekstra, H. J. Bergveld and M. C. Donkers, "Range Maximisation of Electric Vehicles through Active Cell Balancing using Reachability Analysis," in *2019 American Control Conference (ACC)*, 2019.
- [7] L. A. Perișoară, I. C. Guran and D. C. Costache, "A Passive Battery Management System for Fast Balancing of Four LiFePO₄ Cells," in *IEEE 24th International Symposium for Design and Technology in Electronic Packaging (SIITME)*, 2008.
- [8] Amin, K. Ismail, A. Nugroho and S. Kaleg, "Passive balancing battery management system using MOSFET internal resistance as balancing resistor," in *2017*

International Conference on Sustainable Energy Engineering and Application (ICSEEA), 2017.

- [9] K. Vitols, "Efficiency of LiFePO₄ battery and charger with passive balancing," in *2015 IEEE 3rd Workshop on Advances in Information, Electronic and Electrical Engineering (AIEEE)*, 2015.
- [10] D. G. Elvira, H. Valderrama Blavi, J. M. Bosque Moncusí, A. Cid Pastor, J. A. Garriga Castillo and L. Martínez Salamero, "Active Battery Balancing Via a Switched DC/DC Converter: Description and Performance Analysis," in *16th Conference on Electrical Machines, Drives and Power Systems (ELMA)*, 2019.
- [11] Y. J. Park, M. K. Kim, H. S. Kim and B. M. Lee, "Risk assessment of lithium-ion battery explosion: chemical leakages," *Journal of Toxicology and Environmental Health*, vol. 21, no. 6, pp. 370-381, 2018.
- [12] J. Qi and D. Dah-Chuan Lu, "Review of battery cell balancing techniques," in *Australasian Universities Power Engineering Conference (AUPEC)*, 2014.
- [13] M. Räber, D. Hink, A. Heinzelman and D. O. Abdeslam, "A Novel Non-Isolated Active Charge Balancing Architecture for Lithium-Ion Batteries," in *IEEE 27th International Symposium on Industrial Electronics (ISIE)*, 2018.
- [14] L. Zheng, J. Zhu and G. Wang, "A comparative study of battery balancing strategies for different battery operation processes," in *2016 IEEE Transportation Electrification Conference and Expo (ITEC)*, 2016.
- [15] X. Wei and B. Zhu, "The research of vehicle power Li-ion battery pack balancing method," in *2009 9th International Conference on Electronic Measurement Instruments*, 2009.
- [16] A. Ziegler, D. Oeser, B. Arndt and A. Ackva, "Comparison of Active and Passive Balancing by a Long Term Test Including a Post-Mortem Analysis of all Single Battery Cells," in *2018 International IEEE Conference and Workshop in Óbuda on Electrical and Power Engineering (CANDO-EPE)*, 2018.

- [17] J. Ouyang, P. Zhang, S. Wang and H. Li, "Active balancing charging module with continuous and controllable isolation for battery management system," in *2017 IEEE Electrical Design of Advanced Packaging and Systems Symposium (EDAPS)*, 2017.
- [18] G. L. Plett, *Battery Management Systems, Volume II: Equivalent-Circuit Methods*, 1st ed., Artech House, 2015.
- [19] V. Pham, V. Duong and W. Choi, "A Low Cost and Fast Cell-to-Cell Balancing Circuit for Lithium-Ion Battery Strings," *Journal of Electronics*, vol. 9, p. 248, 2020.
- [20] S. Steinhorst and M. Lukasiewicz, "Formal approaches to design of active cell balancing architectures in Battery Management Systems," in *2016 IEEE/ACM International Conference on Computer-Aided Design (ICCAD)*, 2016.
- [21] C. Piao, Z. Wang, J. Cao, W. Zhang and S. Lu, "Lithium-Ion Battery Cell-Balancing Algorithm for Battery Management System Based on Real-Time Outlier Detection," *Mathematical Problems in Engineering*, vol. 2015, pp. 1-12, 2015.
- [22] M. Chen and G. Rincón-Mora, "Accurate Electrical Battery Model Capable of Predicting Runtime and I-V Performance," *IEEE Transactions on Energy Conversion*, vol. 21, pp. 504-511, 2006.
- [23] X. Lin, H. Perez and S. Mohan, "A lumped-parameter electro-thermal model for cylindrical batteries," *Journal of Power Sources*, vol. 257, pp. 1-11, 2014.
- [24] Z. He, M. Gao, J. Xu and Y. Liu, "Battery Model Parameters Estimation with the Sigma Point Kalman Filter," in *2009 International Conference on Artificial Intelligence and Computational Intelligence*, 2009.
- [25] M. Gao, Y. Liu and Z. He, "Battery state of charge online estimation based on particle filter," in *2011 4th International Congress on Image and Signal Processing*, 2011.
- [26] B. Schweighofer, K. Raab and G. Brasseur, "Modeling of high power automotive batteries by the use of an automated test system," *IEEE Transactions on Instrumentation and Measurement*, vol. 52, pp. 1087-1091, 2003.

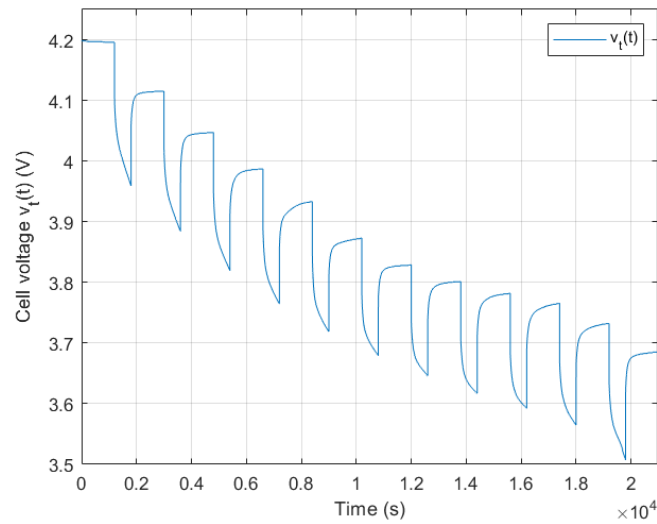
- [27] L. Gao, S. Liu and R. Dougal, "Dynamic lithium-ion Battery model for system simulation," *IEEE Transactions on Components and Packaging Technologies*, vol. 25, pp. 495-505, 2002.
- [28] M. Glass, "Battery electrochemical nonlinear/dynamic SPICE model," in *IECEC 96. Proceedings of the 31st Intersociety Energy Conversion Engineering Conference*, Washington, 1996.
- [29] S. Buller, M. Thele, R. De Doncker and E. Karden, "Impedance-based simulation models of supercapacitors and Li-ion batteries for power electronic applications," *IEEE Transactions on Industry Applications*, vol. 41, no. 3, pp. 742-747, 2005.
- [30] P. Baudry, M. Neri, M. Gueguen and G. Lonchamp, "Electro-thermal modelling of polymer lithium batteries for starting period and pulse power," *Journal of Power Sources*, vol. 54, no. 2, pp. 393-396, 1995.
- [31] L. Benini, G. Castelli, A. Macii, E. Macii, M. Poncino and R. Scarsi, "Discrete-time battery models for system-level low-power design," *IEEE Transactions on Very Large Scale Integration (VLSI) Systems*, vol. 9, no. 5, pp. 630-640, 2001.
- [32] S. C. Hageman, "Simple PSpice models let you simulate common battery types," *Electronic Design News*, vol. 38, pp. 117-129, 1993.
- [33] S. Gold, "A PSPICE macromodel for lithium-ion batteries," in *The Twelfth Annual Battery Conference on Applications and Advances*, Long Beach, USA, 1997.
- [34] C. Bonfiglio and W. Roessler, "A cost optimized battery management system with active cell balancing for lithium ion battery stacks," in *2009 IEEE Vehicle Power and Propulsion Conference*, 2009.
- [35] W. Huang and J. A. Abu Qahoug, "Energy Sharing Control Scheme for State-of-Charge Balancing of Distributed Battery Energy Storage System," *IEEE Transactions on Industrial Electronics*, vol. 62, no. 5, pp. 2764-2776, 2015.
- [36] C. Zun, S. Park and H. Mok, "New Cell Balancing Charging System Research for Lithium-ion Batteries," *Energies*, vol. 13, no. 6, p. 1393, 2020.

- [37] S. Wu, H. Chen and C. Chien, "A Novel Active Cell Balancing Circuit and Charging Strategy in Lithium Battery Pack," *Energies*, vol. 12, no. 23, p. 4473, 2019.
- [38] T. Yang, M. Yu and F. Fang, "State-of-charge balancing control for battery energy storage system based on event-triggered scheme," *Applied Physics A: Materials Science & Processing*, vol. 125, no. 5, 2019.
- [39] C. H. Lin, H. Y. Chao, C. M. Wang and M. H. Hung, "Battery management system with dual-balancing mechanism for LiFePO₄ battery module," in *TENCON 2011 - 2011 IEEE Region 10 Conference*, 2011.
- [40] J. Han, S. Yang, X. Liu and W. Yang, "An Active Direct Cell-to-Cell Balancing Circuit in Continuous Current Mode for Series Connected Batteries," *Energies*, vol. 12, no. 20, p. 3978, 2019.
- [41] R. K. Vardhan, T. Selvathai, R. Reginald and P. Sivakumar, "Modelling of Multi Inductor-based Balancing of Battery Pack for Electrical Mobility," *Defence Science Journal*, vol. 69, no. 3, p. 266, 2019.
- [42] A. Farzan Moghaddam and A. Van de Bossche, "A Ćuk Converter Cell Balancing Technique by Using Coupled Inductors for Lithium-Based Batteries," *Energies*, vol. 12, no. 15, p. 2881, 2019.
- [43] S. Narayanaswamy, S. Park, S. Steinhorst and S. Chakraborty, "Multi-Pattern Active Cell Balancing Architecture and Equalization Strategy for Battery Packs," in *2018 ACM/IEEE International Symposium on Low Power Electronics and Design*, 2018.
- [44] L.-R. Chen, "Design of Duty-Varied Voltage Pulse Charger for Improving Li-Ion Battery-Charging Response," *IEEE Transactions on Industrial Electronics*, vol. 56, pp. 480-487, 2009.
- [45] B. Bole, C. Kulkarni and M. Daigle, "Adaptation of an Electrochemistry-based Li-ion Battery Model to Account for Deterioration Observed Under Randomized Use," *PHM 2014 - Proceedings of the Annual Conference of the Prognostics and Health Management Society 2014*, 2014.

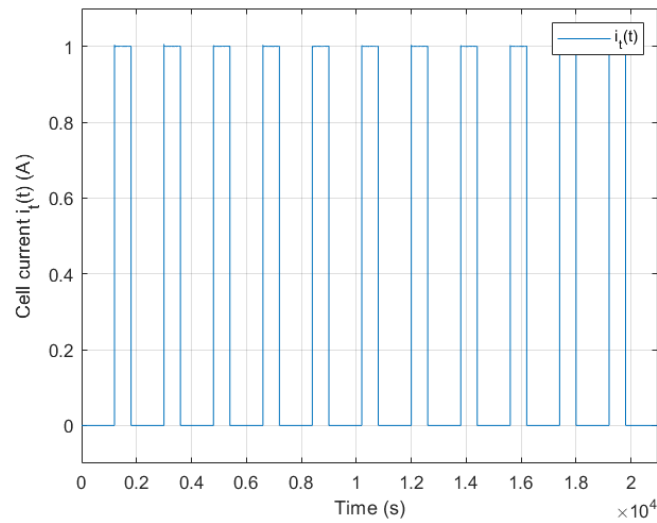
- [46] M. Murshadul, M. A. Hannan and A. Mohamed, "Charging and discharging model of lithium-ion battery for charge equalization control using particle swarm optimization algorithm," *Journal of Renewable and Sustainable Energy*, vol. 8, no. 6, 2016.
- [47] D. W. Hart, Power Electronics, New York, USA: McGraw-Hill, 2011.
- [48] K. Hashimoto, T. Okuda and T. Hikiyara, "A Flyback Converter with SiC Power MOSFET Operating at 10 MHz: Reducing Leakage Inductance for Improvement of Switching Behaviors," in *2018 International Power Electronics Conference (IPEC-Niigata 2018 -ECCE Asia)*, Niigata, 2018.
- [49] D. W. Hart, Power Electronics, Valparaíso, Indiana: McGraw-Hill, 2011.
- [50] A. S. Raj, K. P. Guruswamy, C. Vijay, A. M. Siddeshwar and C. M. Maheshan, "Modelling of flyback converter using state space averaging technique," in *2015 IEEE International Conference on Electronics, Computing and Communication Technologies (CONECCT)*, 2015.
- [51] Texas Instruments, "Design a second-stage filter for sensitive applications," Texas Instruments, 18 Jan 2018. [Online]. Available: https://e2e.ti.com/blogs_/b/powerhouse/posts/design-a-second-stage-filter-for-sensitive-applications. [Accessed 27 March 2021].
- [52] S. Skogestad, "Probably the best simple PID tuning rules in the world," *Journal of Process Control*, 2001.
- [53] E. P. Agency, "EPA Nonregulatory Nonroad Duty Cycles," [Online]. Available: <https://www.epa.gov/moves/epa-nonregulatory-nonroad-duty-cycles>. [Accessed 25 08 2020].

Appendix I. Cell model parameter estimation

Each of the datasets contains a series of 1 A pulsed current reference discharge cycles to allow cell characterization and aging observation after every 50 random walk (RW) cycles [45]. An example of reference discharge cycle can be seen in Figure 31. To estimate the parameters of the battery cells, the first cycle is extracted from every dataset and fed into a parameter estimation algorithm.



(a)



(b)

Figure 31. (a) Cell terminal voltage when discharged under a reference pulsed current cycle, and (b) reference pulsed current discharge cycle.

The parameter estimation algorithm is based on the comparison of the response of an equivalent circuit implemented as a SimScape™ model (shown in Figure 32) loaded with default parameters against the voltage and current data extracted from the datasets. First, the VOC and R0 parameters are initially estimated by analyzing only the voltage profile. Second, the time constants of the RC circuits are initially calculated using a curve fitting function over the pulse relaxation section at each SoC step. Then, both VOC and Rx (resistance value for each RC branch) are estimated using a linear systems approach. Finally, the parameters are fitted using the *Simulink™ Design Optimization* facility available in Simulink™.

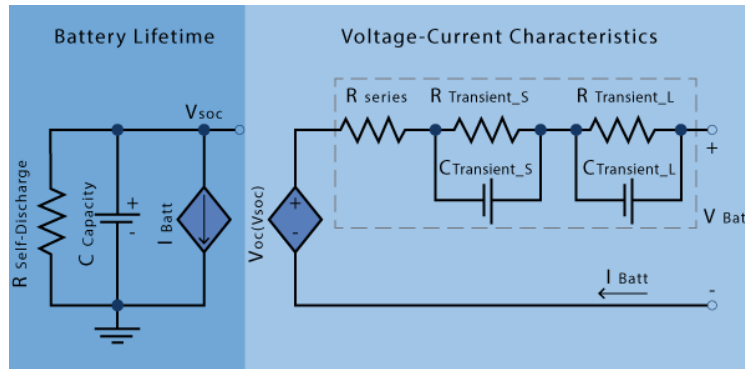


Figure 32. Equivalent circuit cell model used for electrical parameter estimation.

The parameter estimation algorithm comprises the following stages:

1. Loading and preprocessing data: First, data is loaded into the object psObj, which contains the current and voltage, as well as the time vector for the data of the dataset. Second, the data is processed to identify the beginning and the end of each discharge pulse (Figure 33). This information will be later used for parameter estimation. In this stage, the number of desired RC branches is specified. For this algorithm to work, the last discharge pulse must have been completed, in other words, the current vector must end with a 0 value.

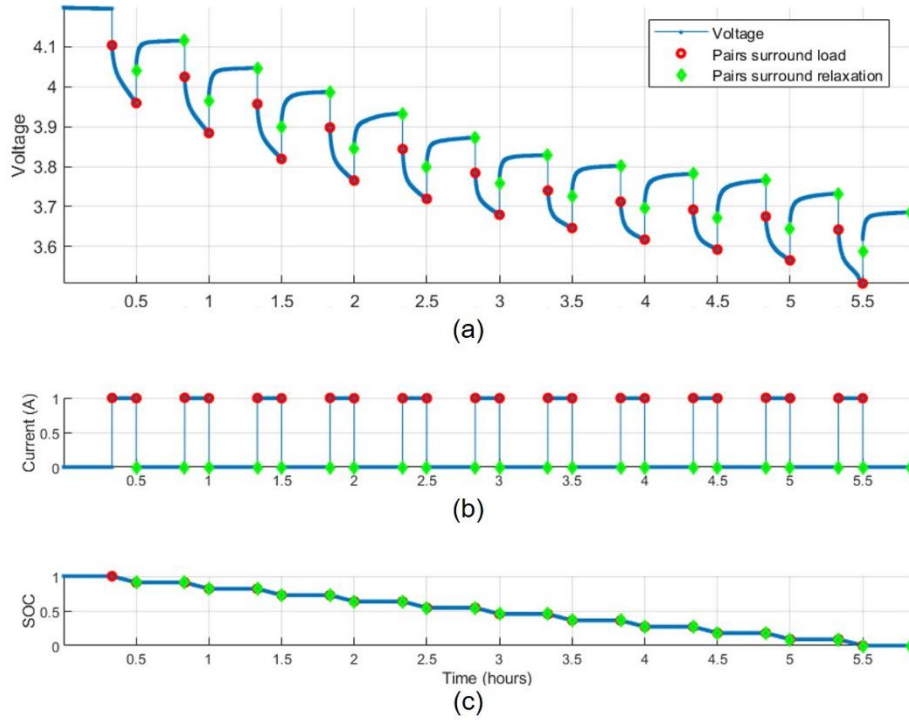


Figure 33. (a) Cell terminal voltage when discharged under reference discharge current cycle, (b) reference discharge current cycle, and (c) cell SoC when discharged under reference discharge current cycle. Red dots limit section of curves corresponding to periods of discharge, while green dots limit section of curves corresponding to rest periods.

2. Initialization to default parameters: The object and models are then loaded with the following default parameters:
 - $VOC = 4 \text{ V}$
 - $R0 = 0.05 \text{ } \Omega$
 - $R1 = R2 = R3 = 0.001 \text{ } \Omega$
 - $T1 = 5 \text{ s}$, $T2 = 100 \text{ s}$, $T3 = 500 \text{ s}$
3. Estimation of the initial VOC: This step inspects the voltage obtained immediately before and after applying the current pulse to determine the VOC and series resistance $R0$, whose trajectories are shown in Figure 34. Note that this figure corresponds to the parameter estimation of an ECM with 2 RC branches.

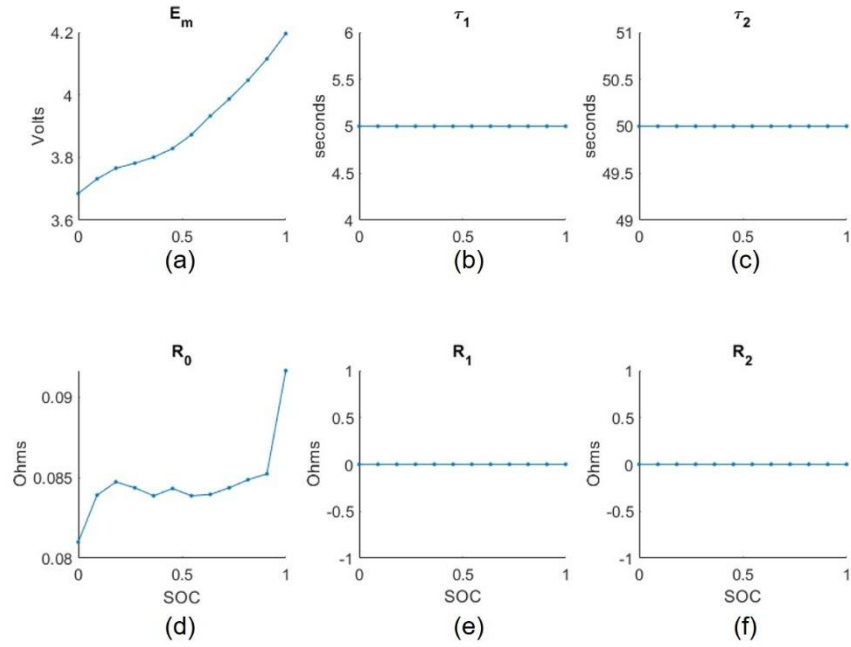


Figure 34. Initial estimation of (a) VOC and (d) series resistance R_0 against SoC. Initial values for (b) time constant 1, (c) time constant 2, (e) resistor R_1 , and (f) resistor R_2 are also shown.

4. Estimation of the initial TC: Applying a curve fitting function on the relaxation curve (after the discharge pulse has been stopped), the evolution of the initial estimations for the time constants are calculated as depicted in Figure 35.

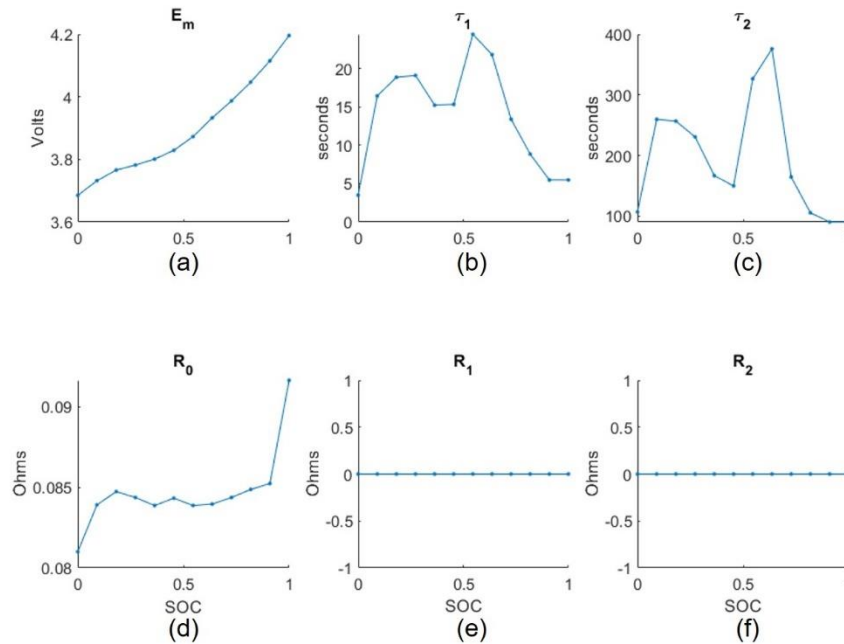


Figure 35. Initial estimation of (a) VOC and (d) series resistance R_0 against SoC. (b) and (c) show the trajectories for time constants 1 and 2 after initial estimation under curve fitting against SoC, while (e) and (f) show the initial guess for R_1 and R_2 .

5. Estimation of R_x : The program estimates the resistance values of each RC branch, according to the time constants obtained and considering a linear system. Updated resistance values are shown in Figure 36.

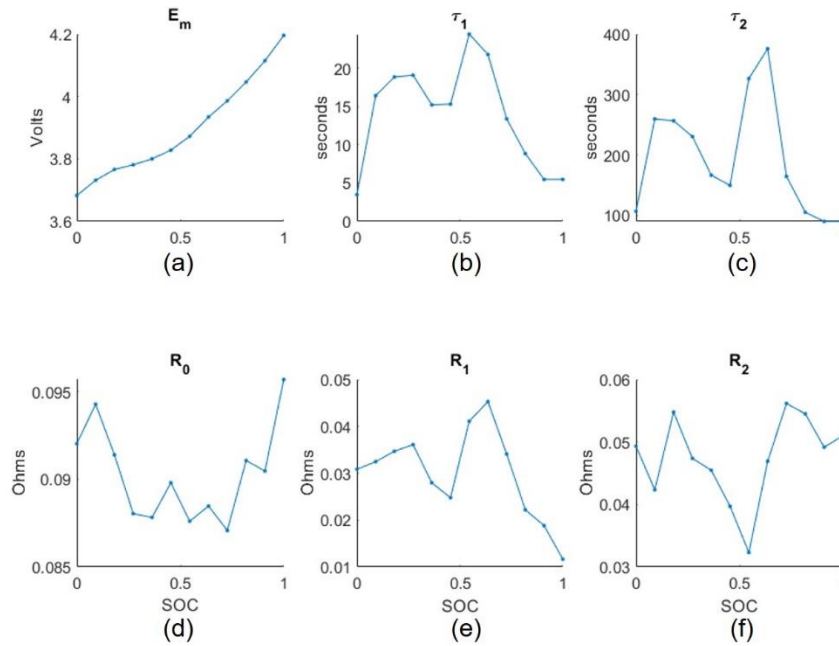


Figure 36. Initial estimation of (a) VOC, (b) time constant 1, (c) time constant 2, (d) series resistor R_0 , (e) resistance R_1 , and (f) resistance R_2 against SoC, considering a linear system.

6. Simulink™ Design Optimization: Using the previous parameters as initial conditions, the *Simulink™ Design Optimization* package is run through parallel computing to fit the response of the model to the data from the dataset. The final parameter values are shown in Figure 37.

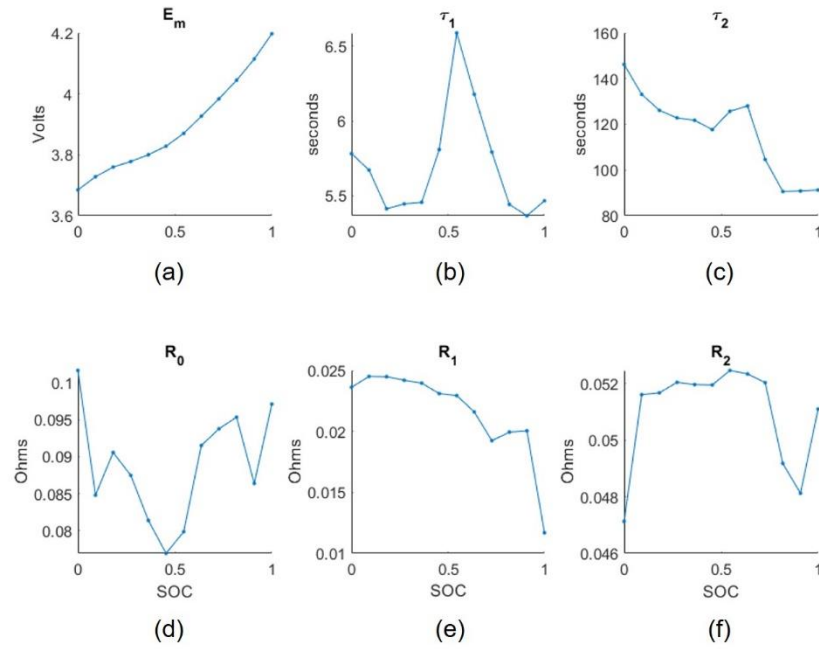


Figure 37. Final parameters of (a) VOC, (b) series resistance R_0 , (c) time constant 1, (d) resistance 1, (e) time constant 2, and (f) resistance 2 against SoC, after design optimization.

7. Creation of look-up tables: The parameters generated through the algorithm are stored into 1D look-up tables, which are ready to be used in other simulations.

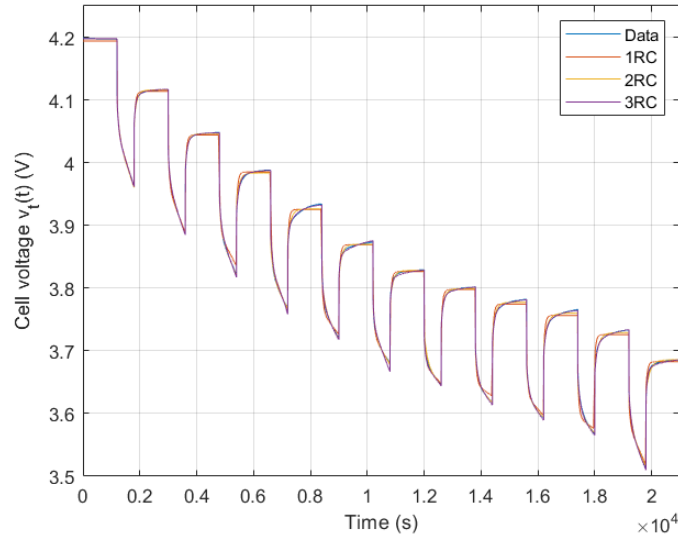
Table 12 summarizes the parameters obtained from the parameter estimation algorithm for the RW4 cell with 3 RC branches. The values show in the table correspond to the individual look up tables, that were generated after analyzing the RW4 cell data under the parameter estimation algorithm. Note how the first RC branch has a smaller time constant when compared to the second and third RC branches. The nonlinearity of the parameters, others than VOC, can also be observed.

Table 12. Electrical parameters obtained from the electrical parameter estimation for a 3RC ECM model.

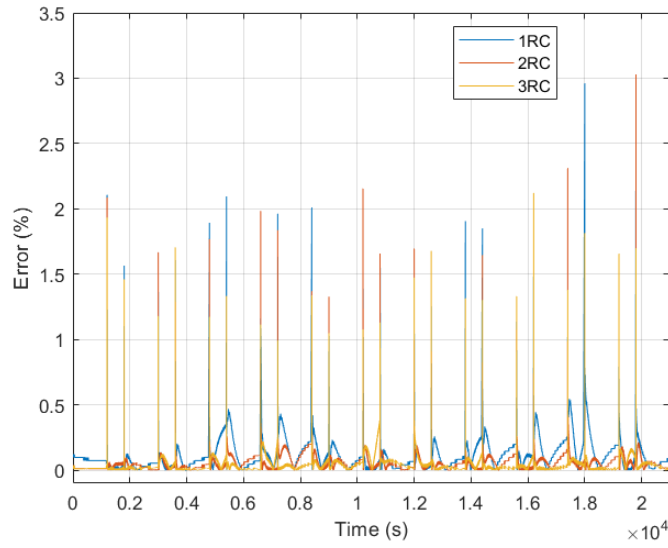
SoC	VOC (V)	R_0 (Ω)	R_1 (Ω)	C_1 (F)	R_2 (Ω)	C_2 (F)	R_3 (Ω)	C_3 (F)
0	3.6888	0.1002	0.0153	80.0089	0.0452	1130.3306	0.0190	36329.0063
0.0909	3.7390	0.0840	0.0148	83.3790	0.0475	1520.0583	0.0419	16943.4645
0.1818	3.7671	0.0889	0.0144	84.8834	0.0491	1592.2075	0.0430	12161.7634
0.2727	3.7842	0.0879	0.0149	72.1798	0.0480	1568.4394	0.0313	18984.7273

0.3636	3.8043	0.0827	0.0147	75.6232	0.0476	1449.8805	0.0310	21000.3037
0.4545	3.8318	0.0923	0.0145	78.1657	0.0427	1300.7481	0.0187	38851.8934
0.5455	3.8836	0.0836	0.0144	79.3352	0.0361	1192.7915	0.0315	26986.4577
0.6364	3.9337	0.0886	0.0151	74.9573	0.0335	1256.1722	0.0840	4305.8059
0.7273	3.9888	0.0896	0.0142	74.0637	0.0555	1596.8674	0.0184	24358.4159
0.8182	4.0475	0.0875	0.0143	73.7476	0.0479	1245.3983	0.0128	18634.1056
0.9091	4.1172	0.0853	0.0134	79.1092	0.0404	1131.8346	0.0221	12971.0579
1.0000	4.1976	0.0923	0.0083	134.1446	0.0483	1288.5179	0.0187	29386.8598

The parameters obtained from the estimation have been used to simulate the battery cell with 1, 2 and 3 RC branches. Figure 38 shows the results of simulating the battery using ECMs with a different quantity of RC branches. It can be noted how the results from the simulation with 3 RC branches follow the original data more closely and thus have a smaller error percentage. Figure 39 shows a closeup portion of the cell voltage curve, where it can be observed how well the different RC branches can estimate the dynamic response of the battery cell.



(a)



(b)

Figure 38. Comparison of 1RC, 2RC, and 3RC models showing (a) cell voltage and (b) error percentage when the reference of the discharge pulse is applied to the system.

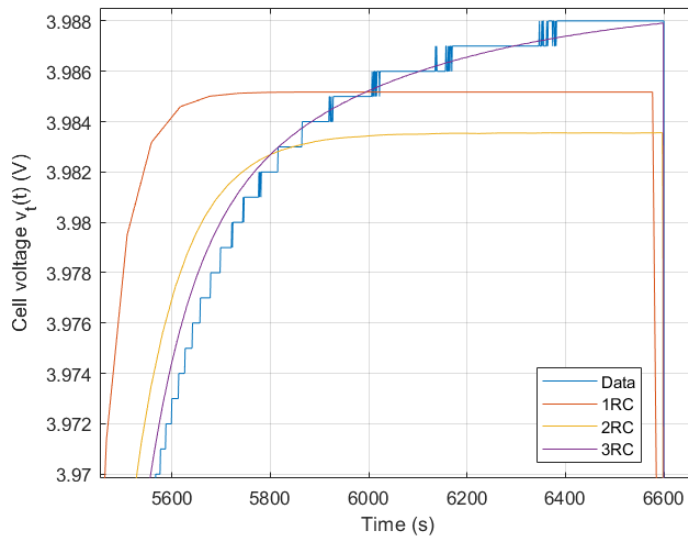


Figure 39. Detail of the comparison of the cell voltage resulting from models with different RC branches.

The maximum and mean errors are summarized in Table 13. As expected, the model with 3 RC branches provides the best fit for this dataset, as both mean and maximum errors are the smallest. It is important to note how the mean error decreases from 1 RC to 2 RC, but it does not change much going from 2 RC to 3 RC. However, the

maximum error shows a significant change. Therefore, it was initially proposed to continue this research by using a 3 RC model.

Table 13. Summary of comparison between 1RC, 2RC, and 3RC models under the reference of the discharge pulsed current.

<i>Characterization</i>	<i>1 RC</i>	<i>2 RC</i>	<i>3 RC</i>
<i>Mean error (%)</i>	0.1254	0.0572	0.0402
<i>Maximum error (%)</i>	2.9606	3.0292	2.1217

To further test the obtained battery models, a RW experiment included in the dataset was used for comparison. The RW experiment consists in exposing the fully charged cell to load pulses with a duration of 5 minutes and a random current value between 0.5 A and 4 A. The RW profile used for validation is shown in Figure 40.

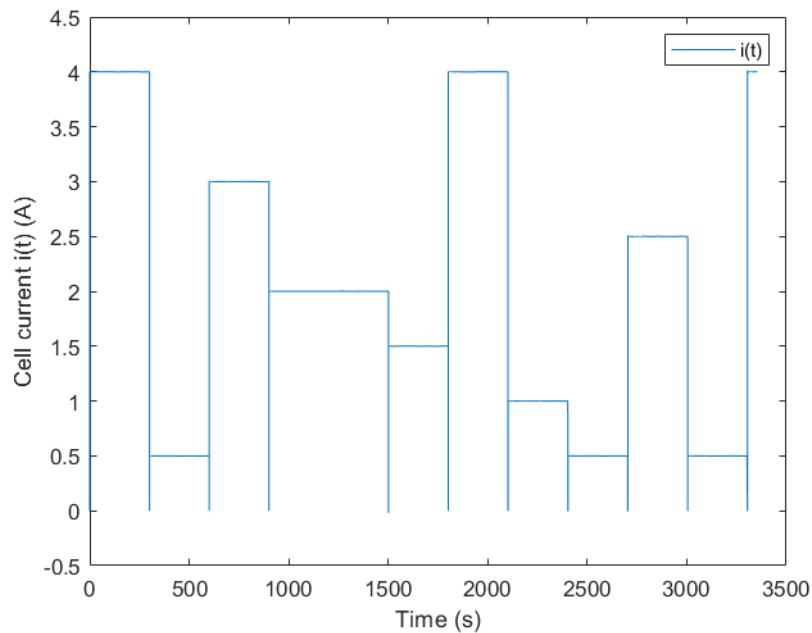
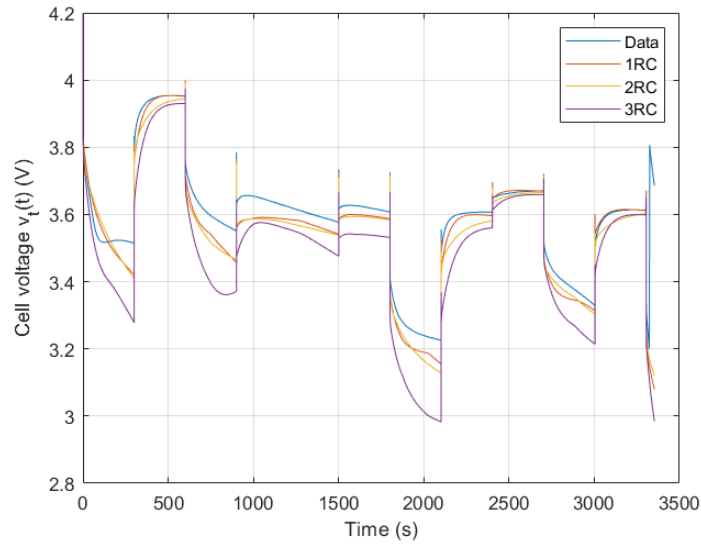
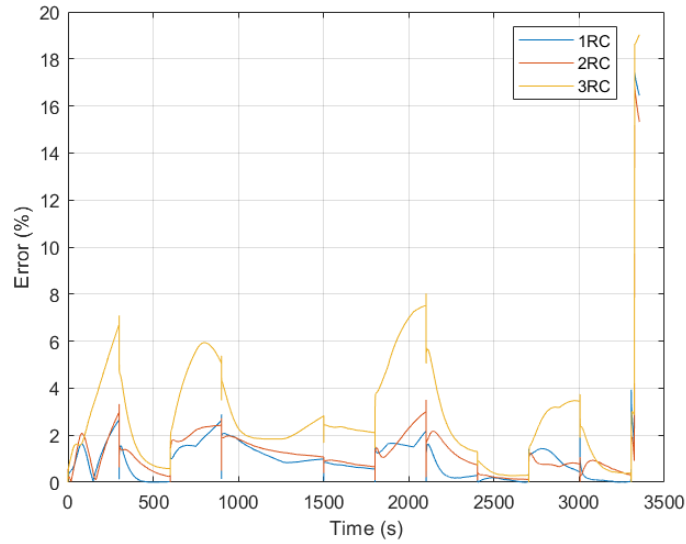


Figure 40. RW current profile showing how current varies between 0 and 4 A at fixed intervals.

The current profile was loaded into each battery model to observe their response. This information was then compared to the values in the dataset to calculate the mean and maximum errors.



(a)



(b)

Figure 41. Comparison of 1RC, 2RC, and 3RC models showing (a) cell voltage and (b) error percentage when a random walk discharge profile is applied to the cells.

Figure 41 shows that the model with the best performance was the circuit with just 1 RC branch. This can be attributed to the fact that the parameter estimation was performed with information pertaining to one discharge rate only. Notice that more RC branches could provide a better fit for characterization experiments where multiple discharge rates are used; however, when used for just one discharge rate, the obtained parameters could be overfitted to the provided profile. This explains why the errors in the

3 RC model are larger than those obtained with the 1 RC model. Therefore, the 1 RC model was deemed more accurate for simulations with varying discharge rates. The errors for each model are summarized in Table 14. Although the maximum error of the 1RC model surpasses 17.4 %, the mean error is just above 1%, which provides accurate simulation results at a lower computational cost.

Table 14. Summary of comparison between 1RC, 2RC, and 3RC models under RW discharge.

<i>RW</i>	<i>1 RC</i>	<i>2 RC</i>	<i>3 RC</i>
<i>Mean error (%)</i>	1.0356	1.1326	2.7060
<i>Maximum error (%)</i>	17.4383	16.8228	19.0284

Appendix II. Simulation of voltage-based passive balancing algorithm

A battery charger along with a passive balancing topology and default balancing algorithm implemented on Stateflow™ were loaded with the parameters found during the parameter estimation to test the performance of the balancing system and of three cells during charging and balancing. The charger considers a CCCV strategy, i.e., a constant charging current is injected into the battery pack until a threshold voltage is reached. A threshold of 11.5 V has been fixed defined for this experiment. Then, the constant voltage strategy is applied. This stage considers a voltage of 12.59 V to fully charge the cells. The resistors for the passive balancing were set to 2.5 Ω , while a charging current of 0.3 C (0.5499 A) was also implemented. The layout of the CCCV charger can be seen in Figure 42.

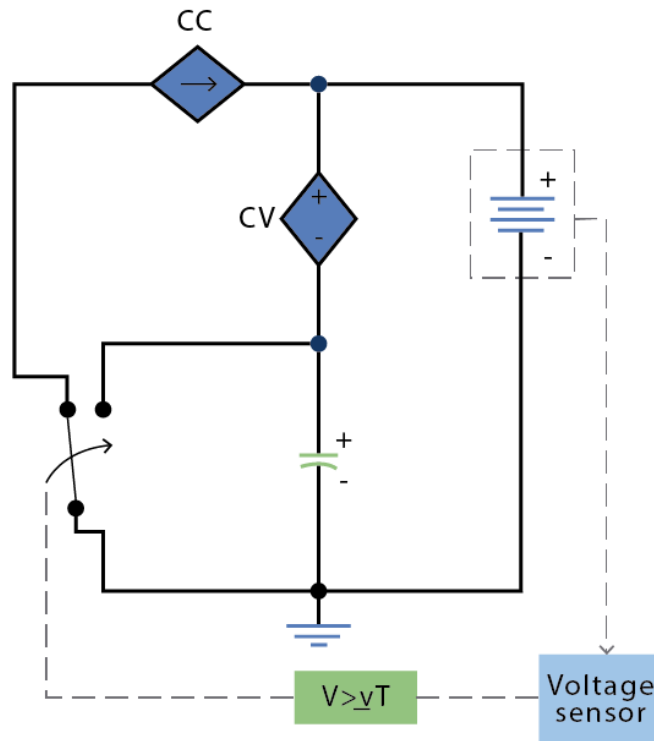


Figure 42. CCCV charger circuit. Solid lines represent electrical flow, while dashed lines represent information flow.

Figure 43 shows the structure of the battery pack and the passive balancing system. R1, R2, and R3 are the bleed resistances, where extra energy from the highest-SoC cells is dissipated. The information of each battery cell is sent to the “Balancing

algorithm” block. This algorithm defines which FET should be activated, i.e. decides which cell needs to unload some energy. The decision is taken by analyzing the VOC of each cell.

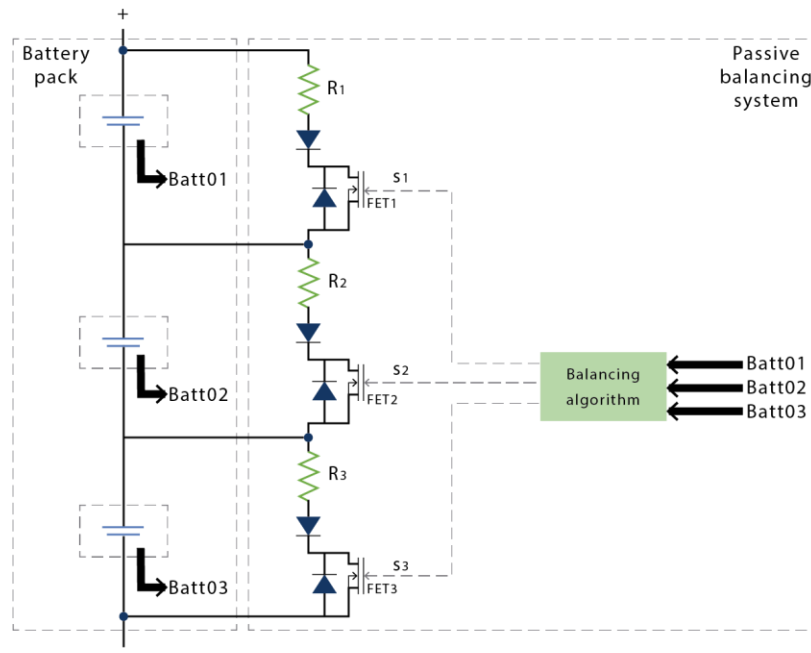


Figure 43. Battery pack comprising 3 individual cells connected to the passive balancing system, which includes a simple balancing algorithm.

The balancing demo provided in Simulink™ includes a simple algorithm developed in Stateflow™, which is shown in Figure 44. This algorithm receives the VOC of each cell after being processed by a sensor (simulated by a transfer function with a large time constant) and decides which cells need to be connected to the resistors to bleed out the excess of energy. This is achieved by turning on the corresponding switching control variables $s1$, $s2$ and $s3$ corresponding to the specific FET attached to each battery cell. The process starts and stops by comparing the largest VOC difference against the ΔV parameter, which has a default value of 0.01 V.

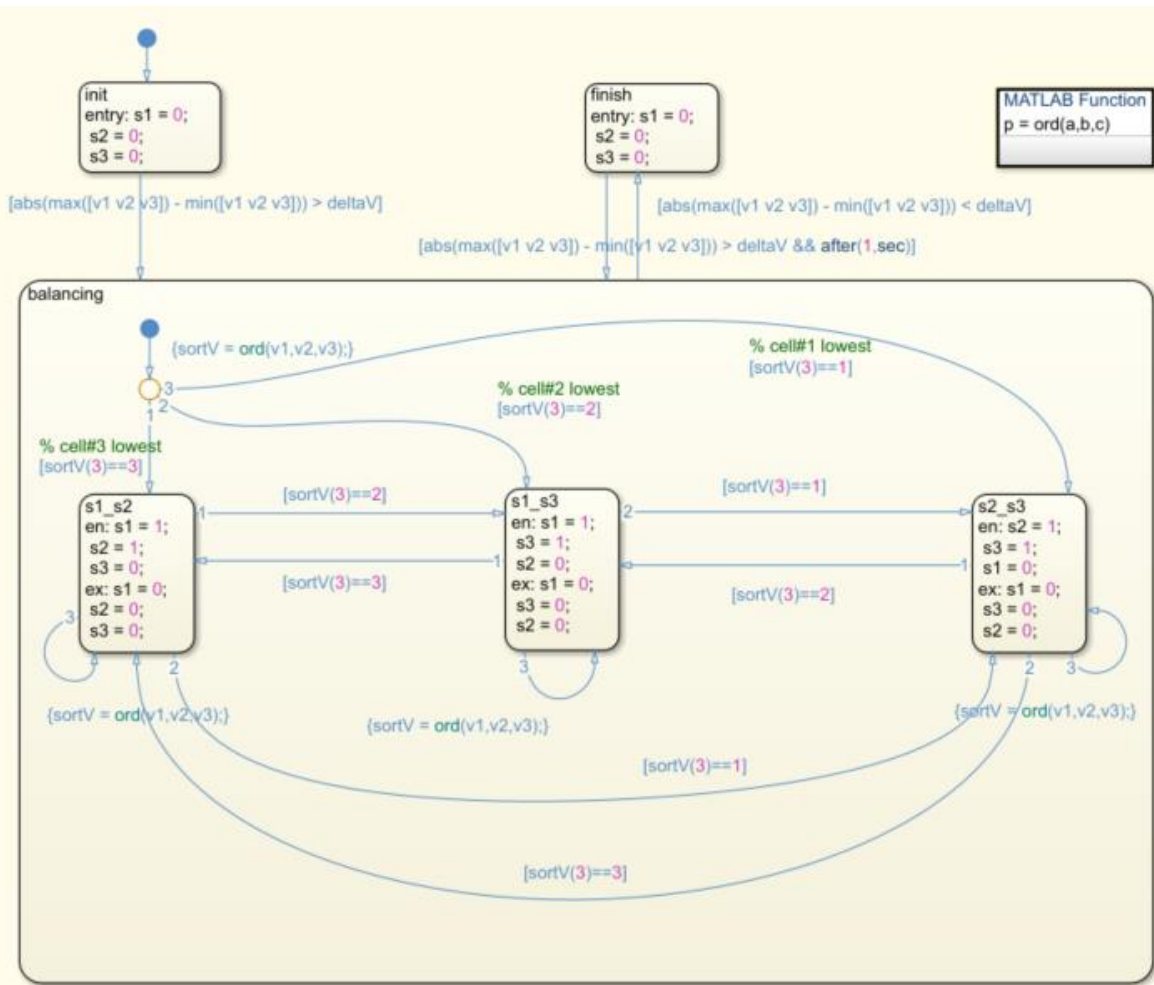


Figure 44. Basic Stateflow™ balancing algorithm for passive balancing considering only VOC.

The algorithm is described as follows:

1. At the *init* stage, the switching control variables s_1 , s_2 and s_3 are initialized to zero. No cell is dissipating extra energy.
2. A comparison between the highest VOC and the lowest one is performed, if the difference is greater than δV , then the algorithm goes into the *balancing* mode.
3. In the *balancing* mode, the cells' VOCs are sorted in a descending order, with the lowest voltage in the last position.
4. Depending on the index of the cell with the lowest voltage, the algorithm can enter to different stages:
 - a. S1_S2: Here the lowest VOC belongs to cell 3. Therefore, the switches for cell 1 and cell 2 are turned on, so they can start dissipating extra energy. After each iteration, VOC values are resorted once again. If a different cell

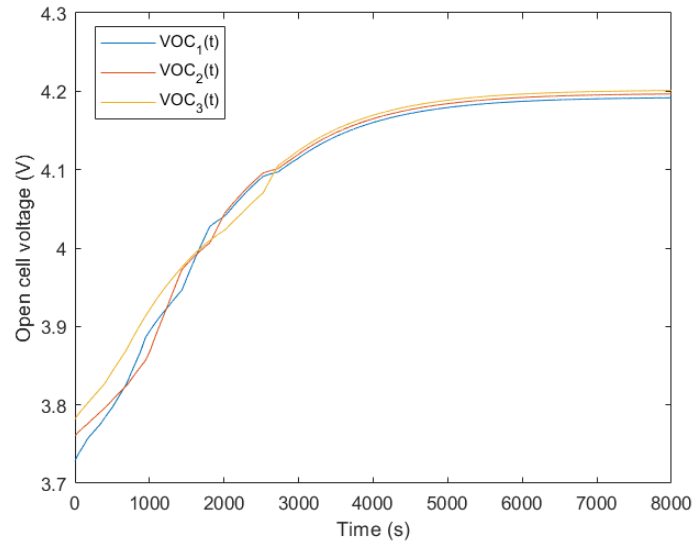
is found to have a lower value, then the algorithm enters the corresponding stage, but first, all switching variables are turned off to stop dissipating energy.

- b. S1_S3: This stage corresponds to cell 2 presenting the lowest VOC. Switches for cells 1 and cell 3 are turned on.
 - c. S2_S3: The algorithm enters this stage when cell 1 was found to have the lowest VOC. Switching variables corresponding to cells 2 and 3 are turned on.
5. After each iteration, the difference between the highest and the lowest VOC values is compared against ΔV once again. If the difference is lower than the threshold, then the algorithm enters to the *finish* stage, where all switches are turned off to stop balancing.
 6. The system can re-enter to the *balancing* mode if the difference between the highest and lowest VOC is larger than ΔV , and at least 1 second has passed since the algorithm went into *finishing* mode, previously.

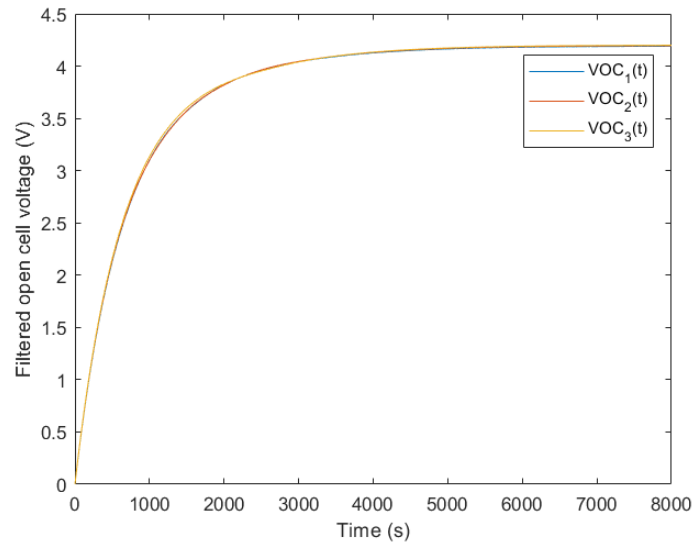
As mentioned before, the values of VOC read by the algorithm are processed by a transfer function that emulates the low-pass filter function of the sensor. This transfer function is given by Eq. 49:

$$\frac{1}{T_{volt} \cdot s + 1} \quad \text{Eq. 49}$$

The T_{volt} parameter has a default value of 600, which causes a very slow response of the signal and prevents the algorithm from oscillating. Figure 45 shows the behavior of the VOC as directly measured from the cells and after being processed by the sensor, respectively. Notice how, even though the actual VOC of each cell is in fact different, the filtered signals show only a very small difference between the VOC of each cell.



(a)



(b)

Figure 45. VOC of the three cells for the (a) unfiltered measurement, and (b) after LPF action of the sensor. Signals processed by the filter show very small variation when compared to each other.

To validate the basic balancing algorithm provided by Simulink™, several simulations were carried out by using varying cell parameters and different initial SoC. The following limitations can be observed in this single factor balancing scheme, which only considers one system state (e.g. VOC):

- The algorithm only considers the VOC state, disregarding the actual SoC and cell terminals voltage.
- No protection for over-current and over-voltage is provided. Cells can easily go beyond the safe limits.
- A somewhat slow response is obtained (around 2 hours for full charge).
- The algorithm tries to send more charge to only one cell at a time, i.e., it forces dissipation of energy in all other cells. This means that even though two cells could have a similar SoC, one of them dissipates energy, while the other is being charged. For example, in a battery pack of 3 cells with SoC of 0.1, 0.11, and 0.2, the last two cells dissipate energy, while only the one with the lowest VOC (and presumably lowest SoC) will be charged.
- As the VOC signal is heavily filtered, some steady-state voltage difference may remain when faced with time-varying cell parameters.
- If cell parameters are not the same between cells, then some cells may reach more than 100% SoC.

The default balancing algorithm has some flaws that may lead to an excessive stress in stronger cells, as well as to differences in final SoC. Therefore, an algorithm that considers cell SoC, along with cell voltage, must be developed to ensure safe operation of the cells and appropriate balance, which is the motivation of the present work.

Curriculum Vitae

Abraham Alberto Martínez Barrón was born in Guaymas, México, on July 1st, 1993. He earned the Bachelor in Mechatronics Engineering degree from the *Instituto Tecnológico y de Estudios Superiores de Monterrey*, Monterrey Campus in May 2015. Since July 2015, he has been working for John Deere in the Electrical Harness Design department. He was accepted in the graduate programs in Energetics Engineering in August 2018.